SANDIA REPORT
SAND2011-2833
Unlimited Release
Printed May 2011

Carbon fiber composite characterization in adverse thermal environments

Joshua A. Hubbard, Alexander L. Brown, Amanda B. Dodd, Sylvia Gomez-Vasquez, and Ciro J. Ramirez

Prepared by
Sandia National Laboratories
Albuquerque, New Mexico 87185 and Livermore, California 94550

Sandia National Laboratories is a multi-program laboratory managed and operated by Sandia Corporation, a wholly owned subsidiary of Lockheed Martin Corporation, for the U.S. Department of Energy's National Nuclear Security Administration under contract DE-AC04-94AL85000.

Approved for public release; further dissemination unlimited.

Issued by Sandia National Laboratories, operated for the United States Department of Energy by Sandia Corporation.

NOTICE: This report was prepared as an account of work sponsored by an agency of the United States Government. Neither the United States Government, nor any agency thereof, nor any of their employees, nor any of their contractors, subcontractors, or their employees, make any warranty, express or implied, or assume any legal liability or responsibility for the accuracy, completeness, or usefulness of any information, apparatus, product, or process disclosed, or represent that its use would not infringe privately owned rights. Reference herein to any specific commercial product, process, or service by trade name, trademark, manufacturer, or otherwise, does not necessarily constitute or imply its endorsement, recommendation, or favoring by the United States Government, any agency thereof, or any of their contractors or subcontractors. The views and opinions expressed herein do not necessarily state or reflect those of the United States Government, any agency thereof, or any of their contractors.

Printed in the United States of America. This report has been reproduced directly from the best available copy.

Available to DOE and DOE contractors from
U.S. Department of Energy
Office of Scientific and Technical Information
P.O. Box 62
Oak Ridge, TN 37831

Telephone: (865) 576-8401
Facsimile: (865) 576-5728
E-Mail: reports@adonis.osti.gov
Online ordering: http://www.osti.gov/bridge

Available to the public from
U.S. Department of Commerce
National Technical Information Service
5285 Port Royal Rd.
Springfield, VA 22161

Telephone: (800) 553-6847
Facsimile: (703) 605-6900
E-Mail: orders@ntis.fedworld.gov
Online order: http://www.ntis.gov/help/ordermethods.asp?loc=7-4-0#online

SAND2011-2833
Unlimited Release
Printed May 2011

Carbon fiber composite characterization in adverse thermal environments

Joshua A. Hubbard, Alexander L. Brown, Sylvia Gomez-Vasquez, and Ciro J. Ramirez
Fire and Aerosol Sciences Department 1532
Sandia National Laboratories
P.O. Box 5800
Albuquerque, New Mexico 87185-MS1135

Amanda B. Dodd
Thermal and Fluid Processes Department 1514
Sandia National Laboratories
P.O. Box 5800
Albuquerque, New Mexico 87185-MS0836

Abstract

The behavior of carbon fiber aircraft composites was studied in adverse thermal environments. The effects of resin composition and fiber orientation were measured in two test configurations: 102 by 127 millimeter (mm) test coupons were irradiated at approximately 22.5 kW/m^2 to measure thermal response, and 102 by 254 mm test coupons were irradiated at approximately 30.7 kW/m^2 to characterize piloted flame spread in the vertically upward direction. Carbon-fiber composite materials with epoxy and bismaleimide resins, and uni-directional and woven fiber orientations, were tested. Bismaleimide samples produced less smoke, and were more resistant to flame spread, as expected for high temperature thermoset resins with characteristically lower heat release rates. All materials lost approximately 20-25% of their mass regardless of resin type, fiber orientation, or test configuration. Woven fiber composites displayed localized smoke jetting whereas uni-directional composites developed cracks parallel to the fibers from which smoke and flames emanated. Swelling and delamination were observed with volumetric expansion on the order of 100% to 200%. The purpose of this work was to provide validation data for SNL's foundational thermal and combustion modeling capabilities.

Acknowledgments

The Cytec composites were obtained from Cytec as samples. We are grateful to them for providing the samples that were so important to this study.

Table of Contents

List of Figures

List of Tables

1 INTRODUCTION

Carbon fiber composite materials are increasingly found in transportation vehicles. The B-2 Spirit Stealth Bomber, F-22 Raptor, and numerous other aircraft and naval vessels have significant quantities. Commercial aviation is increasingly using them as well, with greater than 50% of the structural mass now carbon fiber materials for some new designs. Composite materials have the potential to smolder and burn for extended time periods. As a result, the response of composite materials in adverse thermal environments is of interest. Irradiance levels in hydrocarbon fires can exceed 200 kW/m^2 (Gibson and Hume, 1995); because composite materials increase the fuel loading and potentially the duration of an adverse event it is particularly important to study their behavior. The behavior of more traditional transportation vehicle materials, such as aluminum, is better characterized based on historical testing. Unlike conventional materials, volatile gases are emitted when composite surfaces are exposed to hydrocarbon fires and elevated above the resin's endothermic decomposition temperature. Gases subsequently ignite and begin a series of complex anisotropic heat and mass flows, char formation, cracking and delamination, and chemical decomposition processes within the solid. Measuring and modeling these processes is critical to understand the safety and reliability of composite vessels and their cargo.

Epoxy and bismaleimide are two common resin materials used in composite aircraft. Bismaleimide is a high temperature thermoset resin which exhibits better resistance to combustion and flame spread due to its characteristically lower heat release rate. Char formation is also higher in bismaleimide composites providing an additional layer of thermal insulation to prevent chemical decomposition and the transport of volatile gases to the flame front. Cone calorimetry is used to measure properties like heat release rate and ignition time, and ASTM E 162 specifies a common test configuration used to measure surface flame spread. It is difficult, however, to use these measurements to model more realistic fire scenarios and larger scale systems. The purpose of this work was to provide validation data for the development and validation of SNL thermal and combustion modeling tools for assured safety analysis.

2 EXPERIMENT

The behavior of aircraft composite materials was measured in two thermal test configurations: (a) 102 millimeter (mm) by 127 mm (4 inch by 5 inch) coupons were irradiated by a parallel shroud at 800°C, and (b) 102 mm by 254 mm (4 inch by 10 inch) coupons were irradiated by a perpendicular shroud at 1000°C with an ignition source activated at a coupon temperature of 300°C. The first test configuration will be referred to as the radiant heat test, and the latter will be referred to as the piloted ignition flame spread test. Five test materials were selected: Hexcel woven (fabric) carbon-epoxy, Cytec unidirectional (tape) carbon-epoxy, Cytec fabric carbon-epoxy, Cytec tape carbon-bismaleimide (BMI), and Cytec fabric carbon-bismaleimide, where Hexcel and Cytec were two manufacturers, and epoxy and bismaleimide were resin materials. Cytec BMI and epoxy coupons were laid up according to the following schedule: 0°/45°/90°/135°/0° and coupons were 15 layers thick. Hexcel coupons were laid up at 0°/90° and were also 15 layers thick. Hexcel test coupons were used for scoping tests since these materials had passed their expiration date at the time of cure. The effects of age on resin chemistry and curing are unknown; caution should be used when comparing Hexcel data to data from Cytec samples.

2.1 Radiant Heat Test

Two radiant heat tests were performed on each material. These comprise tests 1-10 in the test matrix (Table 1). A single Hexcel probing test was conducted with a shroud at 1000°C. Otherwise, the thermal response to radiant heat was measured with a shroud at 800°C.

Table 1: Radiant heat and piloted ignition flame spread test matrix

Test Number	Test Configuration	Manufacturer	Fiber	Resin	Shroud Temperature (°C)
1	Radiant heat	Hexcel	fabric	epoxy	800
2	Radiant heat	Hexcel	fabric	epoxy	1000
3	Radiant heat	Cytec	fabric	bmi	800
4	Radiant heat	Cytec	fabric	bmi	800
5	Radiant heat	Cytec	fabric	epoxy	800
6	Radiant heat	Cytec	fabric	epoxy	800
7	Radiant heat	Cytec	tape	bmi	800
8	Radiant heat	Cytec	tape	bmi	800
9	Radiant heat	Cytec	tape	epoxy	800
10	Radiant heat	Cytec	tape	epoxy	800
11	Piloted ignition flame spread	Hexcel	fabric	epoxy	1000
12	Piloted ignition flame spread	Hexcel	fabric	epoxy	1000
13	Piloted ignition flame spread	Cytec	fabric	bmi	1000
14	Piloted ignition flame spread	Cytec	fabric	bmi	1000
15	Piloted ignition flame spread	Cytec	fabric	epoxy	1000
16	Piloted ignition flame spread	Cytec	fabric	epoxy	1000
17	Piloted ignition flame spread	Cytec	tape	bmi	1000
18	Piloted ignition flame spread	Cytec	tape	bmi	1000
19	Piloted ignition flame spread	Cytec	tape	epoxy	1000
20	Piloted ignition flame spread	Cytec	tape	epoxy	1000

The test setup is shown schematically in Figure 1. A 229 mm x 229 mm (9" x 9") Inconel 600 shroud was positioned 140 mm (5 ½") above the front face (i.e., irradiated face) of the test coupon. The shroud was heated by an array of Quartz IR lamps which was 305 mm wide and 305 mm deep (12"x12"). The shroud rested atop 25 mm (1") thick Duraboard LD (rated to 2300°C) which was chamfered to provide a 184 mm x 184 mm (7.25"x7.25") effective radiating surface area.

This configuration gives an approximate view factor from the coupon to the shroud of 0.333 (Ehlert and Smith, 1992). With shroud and coupon temperatures of 800°C and 20°C, respectively, the coupon irradiance is 22.5 kW/m^2 when surface emissivities of the shroud and coupon are included ($\varepsilon = 0.8$). This first order analysis neglects radiative interactions with the surroundings. At a shroud temperature of 1000°C , the irradiance would be approximately 44.7 kW/m^2. Emissivity measurements will be discussed in the Data section.

Two measurement thermocouples (25.4 mm (1") off-center) and two control thermocouples (6.4 mm (0.25") off-center) were attached to the shroud. A 90 second ramp was used to heat the shroud (10°C/s). Five thermocouples were attached to the back side (i.e., insulated side) of the composite coupon with Resbond 989 alumina adhesive. The first was located at the center with the remaining four bisecting the lateral dimensions of the exposed coupon face. Four thermocouples were attached to the front side of the coupon 6.4 mm (0.25") from the perimeter. Thermocouples used in this study were mineral insulated, K Type (Watlow, St. Louis, Missouri). Temperature measurement uncertainty is 0.75% with respect to the measured value (e.g., 2.2°C at 293°C).

The coupon was inset 2.5 mm (0.1") into 25.4 mm (1") thick Duraboard LD. The back side of the coupon was thereby insulated. A 6.4 mm (0.25") thick Zirconia board (Zircar ZAL-45; A10509) mask was cut-out such that the irradiated coupon surface area was 76 mm by 102 mm (3" by 4"). This shielded the coupon edges and also masked the front side thermocouples. The Zirconia board mask was used in tests 1-5. The mask broke due to thermal stresses during test 5, and was subsequently replaced by a ceramic fibrous insulation mat (Fiberfrax 550-K). Exhaust fans were used during the experiments and post-test. Operation of the exhaust fans in the Thermal Test Complex is controllable, however, fans were used irregularly. No fans were operational during tests 1 and 2. One fan was turned on midway between smoking and flaming in test three. One fan was operational during tests 4-9, and all four fans were operational during test 10. This variable should be eliminated if additional tests are conducted.

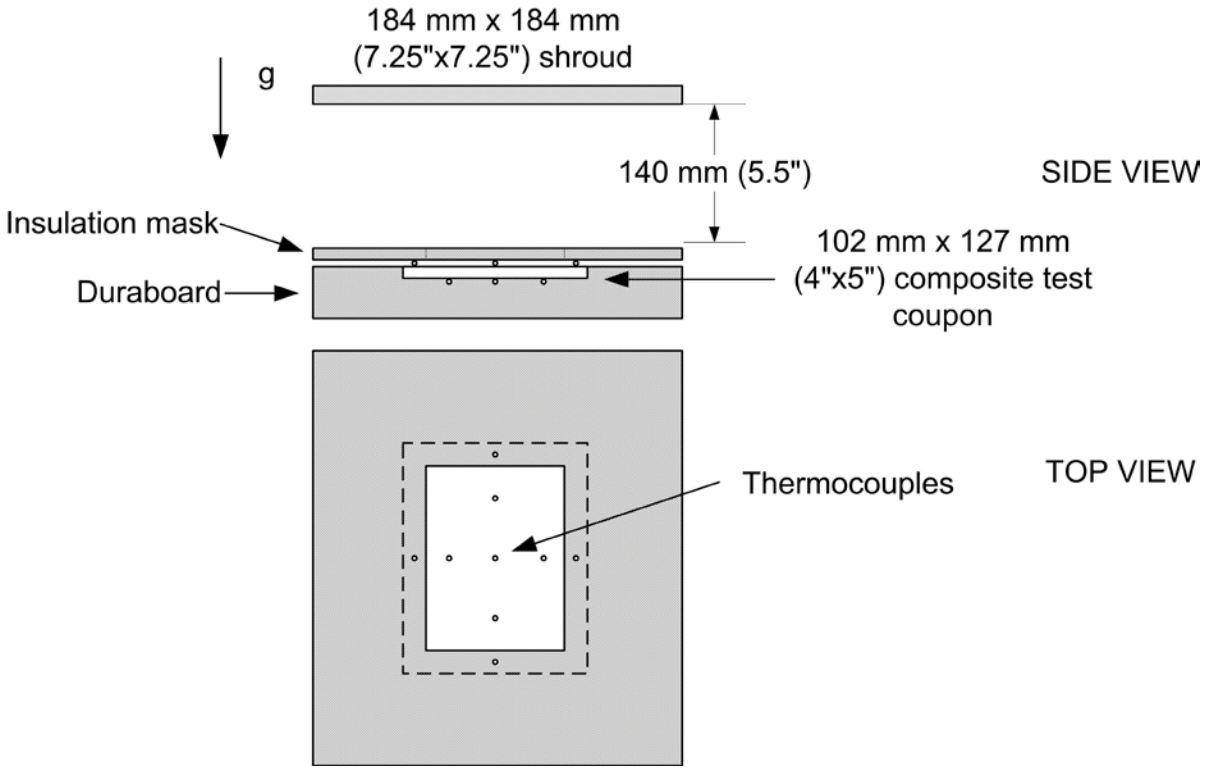

Figure 1: Radiant heat test configuration

2.2 Piloted Ignition Flame Spread Test

Tests 11-20 investigated piloted ignition flame spread. A 102 mm by 254 mm (4" x 10") test coupon was placed perpendicular to a 241 mm by 445 mm (9.5" x 17.5") shroud as shown in Figure 2. The bottom edge of the coupon was 25 mm (1") above the face of the shroud. Similar to the radiant heat tests, a 12.5 mm (0.5") Zirconia board mask was placed over the test coupon to minimize edge effects and mask the front side thermocouples. Five thermocouples were spaced at 38 mm intervals (1.5") along the back side of the test coupon starting 51 mm (2") from the bottom of the coupon. Two thermocouples were placed on the front side of the test coupon 6.4 mm (0.25") from the top and bottom edges of the coupon. The shroud temperature was set to ramp to 1000°C over 120 seconds. A 12 VDC carbide glow plug was used as the ignition source. The bottom edge of the glow plug housing was flush with the bottom exposed edge of the composite coupon. The glow plug was turned on once the composite coupon temperature reached 300°C. A pyrometer was also used to make measurements of temperature. The 51 mm (2") diameter measurement region (pyrometer) was directed at the top of the coupon. The measurement range of the pyrometer was 450°C to 1200°C. A photograph of the test setup is shown in Appendix Figure A.11.1. The view factor from the shroud to the coupon was calculated as 0.036 using the method of Ehlert and Smith (1992). Ignoring radiative interactions with the surroundings, the spatially averaged coupon irradiation is approximately 30.7 kW/m^2 for a shroud temperature of 1000°C. Operation of TTC exhaust fans was uniform during piloted ignition flame spread tests. A single exhaust fan was operational throughout tests 11-20.

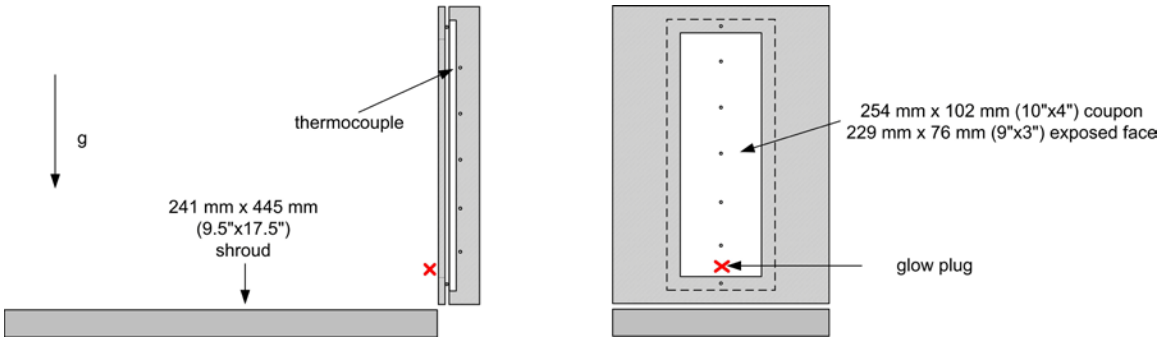

Figure 2: Piloted ignition flame spread test configuration

3 DATA

All elapsed time measurements given here are referenced from the time at which the lamp ramp began. Time measurement uncertainty is ± 2 seconds. Test setup photographs, thermocouple legends, temperature profiles, and pre- and post-test sample photographs are given in Appendix A. For radiant heat tests, the lamps were shut off at the onset of flaming combustion unless otherwise noted. For piloted ignition flame spread tests, the igniter was turned off at the time of ignition.

3.1 Composite Coupon Characteristics

3.1.1 Surface Emissivity

Surface emissivity measurements were made with an SOC 410 DHR Reflectometer with accuracy of 0.001 (Surface Optics Corporation, San Diego, California). Table 2 gives the measured values of directional total emissivity (DTE) and hemispherical total emissivity (HTE). The suffixes 20 and 60 refer to the incidence angle. For instance, DTE20 gives the spectrally averaged emissivity when the sample surface is irradiated from an incidence angle of 20 degrees. The HTE provides a spectrally and directionally integrated emissivity. Each composite material has a rough side and a smooth side. The smooth side was irradiated. However, emissivities were measured on both sides. Each measurement in Table 2 is the average of 3 independent measurements; heterogeneity in the surface is averaged out. Typically, the standard deviation due to surface heterogeneity was less than 0.01. Nominally, DTE20 is greater than DTE60 or HTE, and the rough surface has higher emissivity than the smooth surface. Little difference is observed between BMI and epoxy resins.

Table 2: Surface emissivity measurements of shroud and composite materials

supplier	fiber	resin	smooth surface			rough surface		
			DTE20	DTE60	HTE	DTE20	DTE60	HTE
Shroud			0.82	0.80	0.77			
Hexel	Fabric	Epoxy	0.88	0.83	0.81	0.89	0.84	0.82
Cytec	Fabric	BMI	0.86	0.82	0.80	0.90	0.86	0.84
Cytec	Fabric	Epoxy	0.86	0.81	0.80	0.85	0.81	0.80
Cytec	Tape	BMI	0.85	0.78	0.80	0.88	0.86	0.82
Cytec	Tape	Epoxy	0.86	0.82	0.80	0.90	0.86	0.84

3.2 Radiant Heat and Piloted Flame Spread Tests

3.2.1 Linear expansion

Pre- and post-test coupon dimensions were measured with calipers to an accuracy of 0.001". Pre- and post-test coupon masses were also measured, to an accuracy of 0.1 gram, to evaluate mass loss. Percentage change in thickness is shown in Figure 3. The thickness was measured at the thickest edge location on the composite sample and increased by approximately 99±21% and 191±55%, for fabric and tape composite coupons. Tape composite coupons

expanded significantly more than the fabric coupons. There is considerable scatter in thickness measurements as each value represents the maximum change for each sample and could be significantly larger than the average change. The change in thickness at the center of each coupon may be a better metric. Edges may be more prone to delamination due to the curing and cutting processes (i.e., small coupon size).

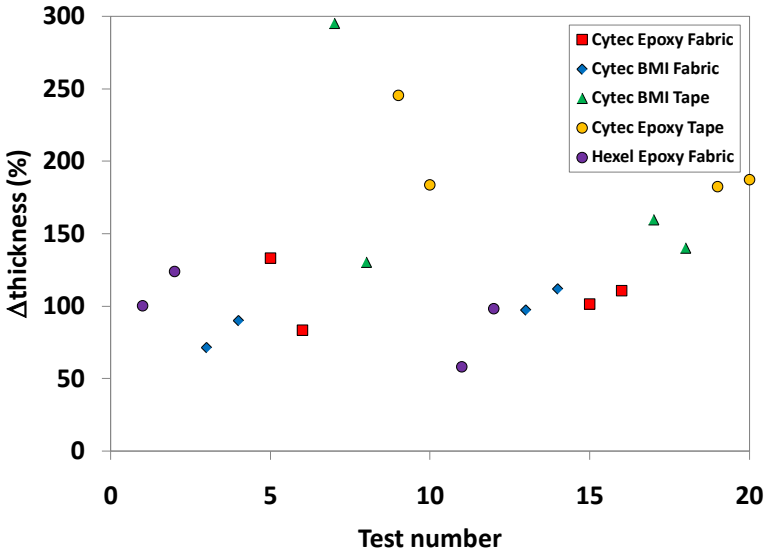

Figure 3: Change in thickness (%) taken at the maximum dimension pre- and post-test for all samples

3.2.2 Mass loss

Percentage changes in mass are shown in Figure 4 and were less dependent on fiber configuration (i.e. tape or fabric). Average mass loss was -25±4% and -19±1% for fabric and tape composite coupons, respectively. End of test condition for tests 1-10 (radiant heat) changed because some composites ignited (1,2,3, and 9). When flaming did not occur, lamps were shut off once the sample temperature profile reached its asymptotic value. In Figure 5, no distinct correlation was found for mass loss as a function of irradiation time. This may imply resin depletion was complete prior to the end of test. Tests 11-20 (piloted ignition flame spread) appear more uniform in terms of mass loss percentage for similar repeated tests, possibly due to more uniform test conditions: lamps were shut off once the flame self-extinguished.

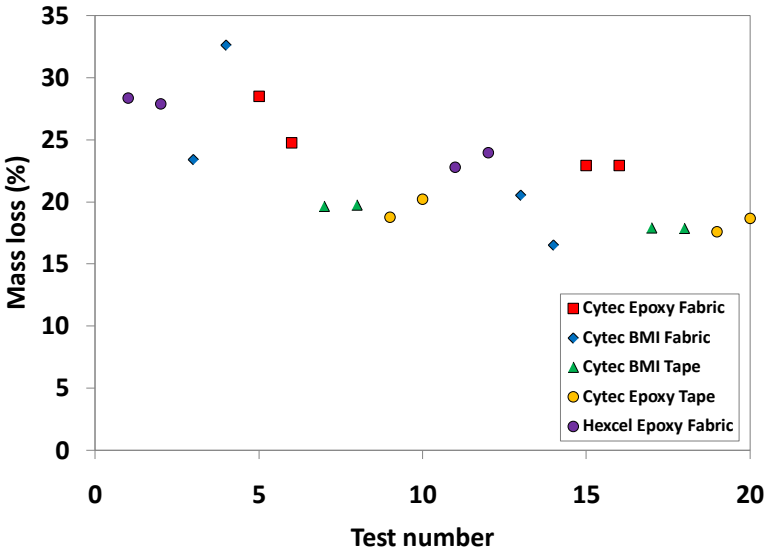

Figure 4: Mass loss (%) for all test samples

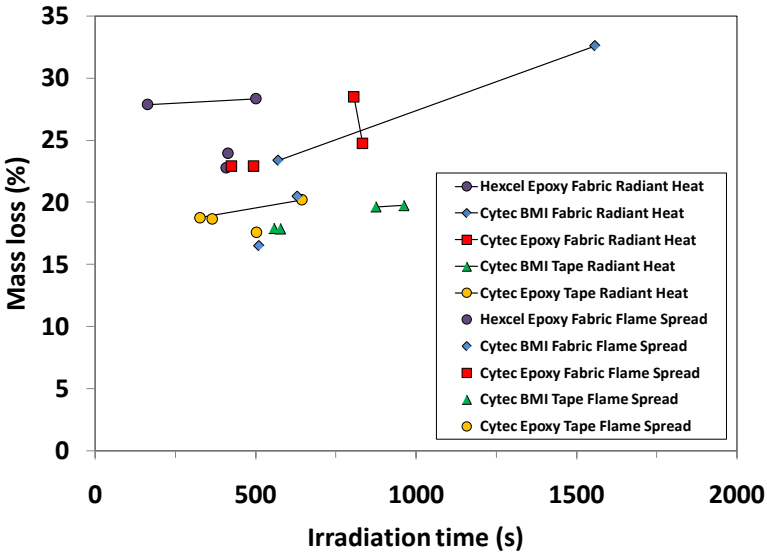

Figure 5: Mass loss (%) as a function of total irradiation time (s)

3.3 Piloted Flame Spread Test

3.3.1 Pre-ignition smoke generation and ignition time

Data for piloted ignition flame spread tests provide more robust comparisons since test conditions (i.e., operation of exhaust fans) and end of test specification (i.e., self-extinguishing) were consistent throughout the test series. The average duration of pre-ignition smoke generation is shown in Figure 6. Error bars give the two replicate test values used to calculate the average. Bismaleimide tape composites appeared to resist ignition for a prolonged period. However, large variability (COV=0.5) in epoxy tape and BMI fabric data obscure any general

trends that may exist. Additional replicate experiments would be preferable to fully examine general trends.

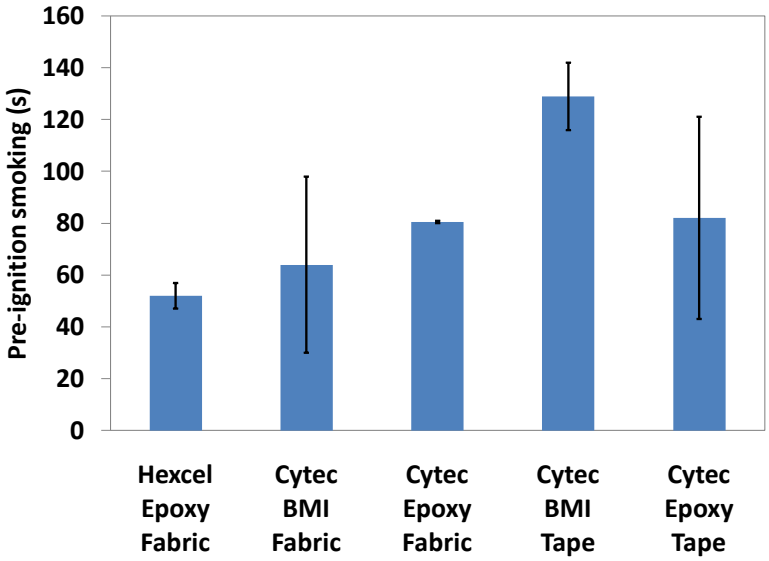

Figure 6: Average duration of pre-ignition smoking (seconds) for piloted ignition flame spread test. Error bars show the range of values since two tests were conducted for each material.

Average ignition times are plotted in Figure 7. Again, variability obscures any significant difference in ignition time.

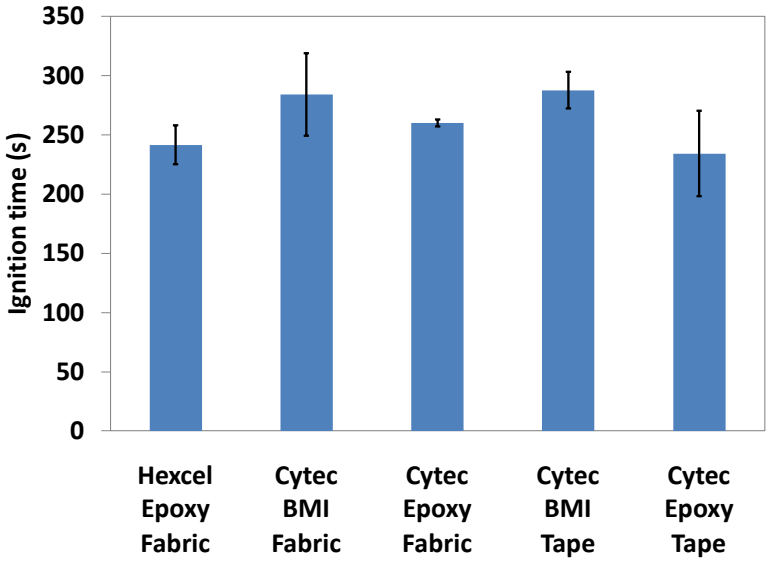

Figure 7: Average ignition time (seconds) for piloted ignition flame spread tests. Error bars show the range of values since two tests were conducted for each material.

3.3.2 Sustained flaming and mass loss

Figures 8 and 9 show the average duration of sustained flaming combustion and percentage mass loss, respectively. Bismaleimide coupons sustained combustion for an average of 129 seconds longer than epoxy coupons. BMI samples should exhibit lower mass loss rates due to characteristically lower heat release rates, increased char formation, and higher resistance to combustion. However, mass loss does not display any discernable trend. This suggests resin depletion was complete at the end of each test and nominally the same for epoxy and BMI.

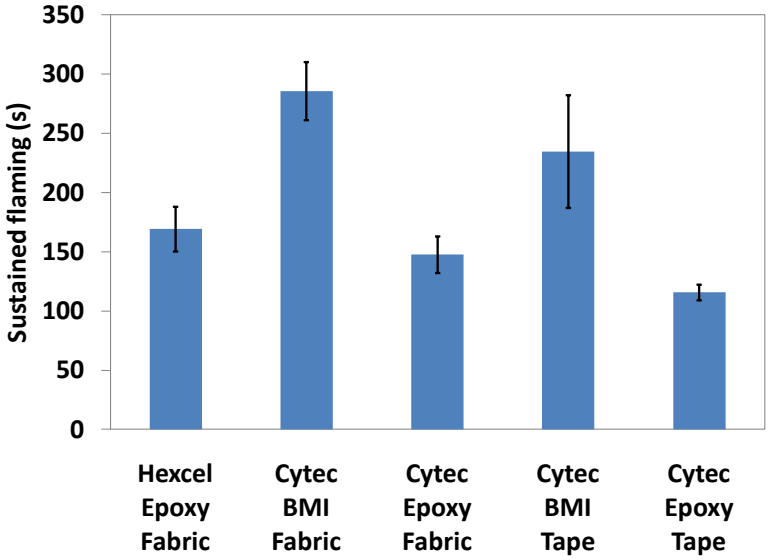

Figure 8: Average duration of sustained flaming (s) for piloted ignition flame spread test. Error bars show the range of values since two tests were conducted for each material.

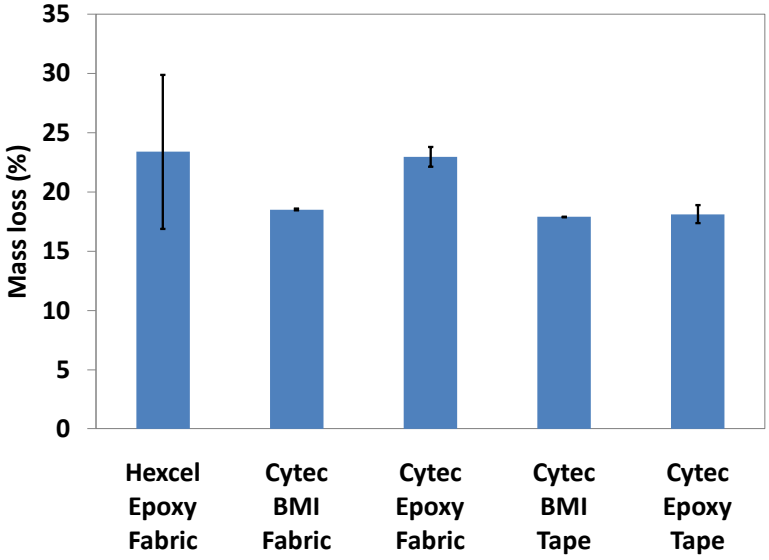

Figure 9: Average mass loss (%) for piloted ignition flame spread test. Error bars show the range of values since two tests were conducted for each material.

4 OBSERVATIONS

4.1 Hexcel Epoxy Fabric, Radiant Heat (Test 1)

Referring to Appendix A, Figures A.1.1 and A.1.3 show test photographs and temperature profiles, respectively, for test 1. During test 1, the shroud was heated to 800°C. The material began smoking at approximately 200 seconds. Shortly thereafter, appreciable coupon swelling was observed. The Zirconia board mask lifted approximately 6 mm (~0.25") in only one corner indicating non-uniform volumetric expansion. This event occurred when the back side temperature was approximately 280°C and coincides with the expected temperature at which resin decomposition begins. During the smoking stage, molten resin bubbles formed on the front side of the coupon. Transition to flaming combustion occurred around 450 seconds when the back side temperature was approximately equal to 400°C. The lamps were shut off at an elapsed time of 500 seconds. Initially the flame was confined to the central portion of the coupon where resin bubbles formed during the smoking stage. The flame spread to cover the coupon uniformly over a period of approximately 60 seconds. The flame was sooty and self-extinguished at an elapsed time of 594 seconds. The flaming period was approximately 144 seconds.

Figure A.1.3(c) shows average front side and back side temperature profiles as well as the average temperature difference. Thermocouples which had apparently detached from the surface or exhibited spurious behavior were excluded from these averages. Off-gassing at the edges, asymmetric expansion, and the resulting lifting of the Zirconia board mask, adds a degree of uncertainty to the front side thermocouple measurements. An air gap could affect measurement uniformity by altering heat transfer in the thermocouple region. Once off-gassing commenced, this could have added a blowing effect (convective heat transfer) over the front side thermocouples if the gasses could not escape laterally through the insulation. This is reflected in the error bars (± 1 standard deviation) in Figure A.1.3(c) which grow to approximately ± 30°C on the front side and ± 15°C on the backside. It is recommended that back side temperature measurements be used for model development and validation.

The physical interpretation of temperature difference should be considered carefully. The irradiated surface temperature measurements (underneath the mask) are less than the backside temperature measurements. However, we know from first principles the exposed front face temperature is greater than the back face temperature. Neglecting phase change and resin decomposition, heat is transferred through the solid, perpendicular to the fibers, from the irradiated face to the insulated face. Front-side thermocouples are masked from irradiation, thus the conduction problem is two-dimensional and heat is transferred laterally (i.e., in the direction parallel to the carbon fibers). Therefore, the thermocouple measurements on the front face of the coupon are not truly indicative of the front face temperature which drives heat conduction through the solid. It is not recommended that front face temperature measurements be used for model validation purposes.

The maximum temperature difference occurred at approximately the same time at which volumetric expansion was observed. This temperature difference is a qualitative measure of the lateral temperature gradient, and thus indicates mechanical stress within the coupon. Edges are insulated and cooler than the center of the coupon thereby creating thermally induced stresses within the material. Sudden expansion occurs when this mechanical stress is larger than the strength of the resin material. After expansion, the temperature difference decreases as would be expected since the coupon is insulated on the back side and the coupon approaches steady-state

conditions. Another inversion (minimum) in temperature difference occurs after the onset of flaming combustion. This is could be the result of additional convective heat transfer over the front side thermocouples or due to the endothermic reaction sustained at the front face during combustion. Pre- and post-test coupon pictures can be seen in Figure A.1.4 where the bubbly resin residue and char formation are emphasized.

4.2 Hexcel Epoxy Fabric, Radiant Heat (Test 2)

A probing test was conducted at a shroud temperature of 1000°C. The coupon quickly began to smoke after 129 seconds and proceeded almost directly to flaming combustion at 143 seconds. Two successive expansions and contractions were observed after 10 seconds of flaming. Billows of smoke escaped laterally during the coupon contractions. A uniform flame covered the coupon surface for approximately 190 seconds. As the flame self-extinguished it was primarily located near the edges of the Zirconia board mask. Figure A.2.1 shows average temperatures and the temperature difference. Flaming combustion occurred when the back side temperature was 220°C. Typically, resin decomposition occurs near 300°C. The maximum temperature difference (lateral temperature gradient) occurs at approximately the same time as mechanical swelling. The absence of resin residue is a clear difference between test 1 and test 2. Pre- and post-test pictures can be seen in Figure A.2.2. The absence of prolonged smoking and off-gassing (prior to flaming combustion) through the front face could be the cause of this difference.

4.3 Cytec Bismaleimide Fabric, Radiant Heat (Test 3)

The onset of smoking occurred near 215 seconds when the back side coupon temperature was approximately 300°C. Initially the smoke was uniform but quickly concentrated into smoke jets with clearly defined origination points. Residue bubbles did not form on the surface. See Figure A.3.2. The Zirconia board mask was attached to the Duraboard with bolts during this test to compress the test fixture. Swelling did occur but the coupon and mask remained vertically constrained. The transition to flaming combustion occurred at approximately 555 seconds and lasted for 130 seconds prior to self-extinguishing. Figure A.3.1(c) shows the average temperature difference reached a maximum prior to swelling as previous tests show. However, the temperature difference becomes negative after the onset of flaming, potentially due to endothermic reactions.

4.4 Cytec Bismaleimide Fabric, Radiant Heat (Test 4)

Smoking and swelling occurred after approximately 205 seconds when the back side coupon temperature reached 300°C. Coupon swelling was strong enough to crack the Zirconia board mask. Several residue bubbles were observed on the surface with smoke jets emanating in close proximity. Smoking ceased at approximately 880 seconds and the lamp array was shut off at 1560 seconds. The transition to flaming combustion was not observed for this test which was unexpected given the results of tests 1-3. The average temperature profiles and temperature difference were similar to test 3. The temperature difference reached a minimum several hundred seconds prior to the cessation of smoking and then approached zero in the asymptotic time limit. This could be an indicator of the blowing effect over the front surface thermocouples.

Volatile gases are emitted from the material during decomposition. Gases emitted from the back side or edges must escape through the insulation, or more likely flow around the edges and over the front face thermocouples. This transport of gases over the thermocouples could alter the heat transfer to each thermocouple effectively "blowing" on the surface and effecting temperature measurements. Figure A.4.2 shows very little surface char or residue on the front face. The top surface layer delaminated from the composite coupon upon disassembly of the test fixture.

4.5 Cytec Epoxy Fabric, Radiant Heat (Test 5)

A new Zirconia board mask was fabricated for test 5. Bolts were not used to compress the coupon since the mask was much larger and the weight was thought to provide sufficient compression without adding the risk of thermal stress and breakage. Smoking and swelling occurred after approximately 165 seconds at a back side coupon temperature of approximately 300°C. Smoke jets and residue bubbles were formed on the surface. Smoking ceased at 660 seconds. This coupon did not transition to flaming combustion. The weight of the Zirconia board mask did cause it to crack down the middle prompting the use of fibrous mat insulation for tests 6-10. Interestingly, Figure A.5.2 shows the surface remained relatively glossy even though residue bubbles formed. Test 3 (Cytec BMI fabric) showed a layer of char formation and test 4, although it was the same material, remained glossy, the difference being test 3 transitioned to flaming combustion. This transition is likely to cause a change in radiative properties of these surfaces.

4.6 Cytec Epoxy Fabric, Radiant Heat (Test 6)

Minor smoking began at an approximate time of 100 seconds, swelling was observed at 180 seconds, and vigorous smoking, residue formation, and smoke jetting began shortly thereafter. The transition to flaming combustion did not occur. Figure A.6.2 shows a post-test side view of the coupon. Significant volumetric expansion is observed.

4.7 Cytec Bismaleimide Tape, Radiant Heat (Test 7)

Test 7 was the first test coupon constructed of uni-directional composite fibers. At approximately 150 seconds a gas pocket developed under the top lamina (seen in Figure A.7.2). Cracks running parallel to the fiber direction grew as the internal pressure increased. These cracks were the locations at which smoke emanated from the test coupon. Later smoke appeared more uniform over the surface and not confined to the locations of cracks. Residues did not form on the irradiated surface and the transition to flaming combustion did not occur.

4.8 Cytec Bismaleimide Tape, Radiant Heat (Test 8)

The results of test 8 were similar to test 7. However, acquisition of thermocouple data was affected by a possible grounding error. These data have been eliminated from Figure A.8.1(a-b) but do affect average temperature profiles in Figure A.8.1(c) by reducing the number of data averaged.

4.9 Cytec Epoxy Tape, Radiant Heat (Test 9)

Smoking and swelling occurred at 130 seconds with a transition to flaming at 290 seconds. Flames only covered one-half the test coupon and self-extinguished after 140 seconds. Figure A.9.2(b) shows a spider web-like pattern not aligned with the fiber direction or cracks. This was likely the result of flaming combustion as it was not seen in test 7 and 8, nor will it be observed in the photographs from test 10.

4.10 Cytec Epoxy Tape, Radiant Heat (Test 10)

Similar to test 9, the process of smoking, swelling, and cracking began at 130 seconds. However, the transition to flaming combustion did not occur. A time sequence of still images is shown in Figure 10. A small bubble appears in the second image. Cracks subsequently grow and smoke begins to emanate from the coupon.

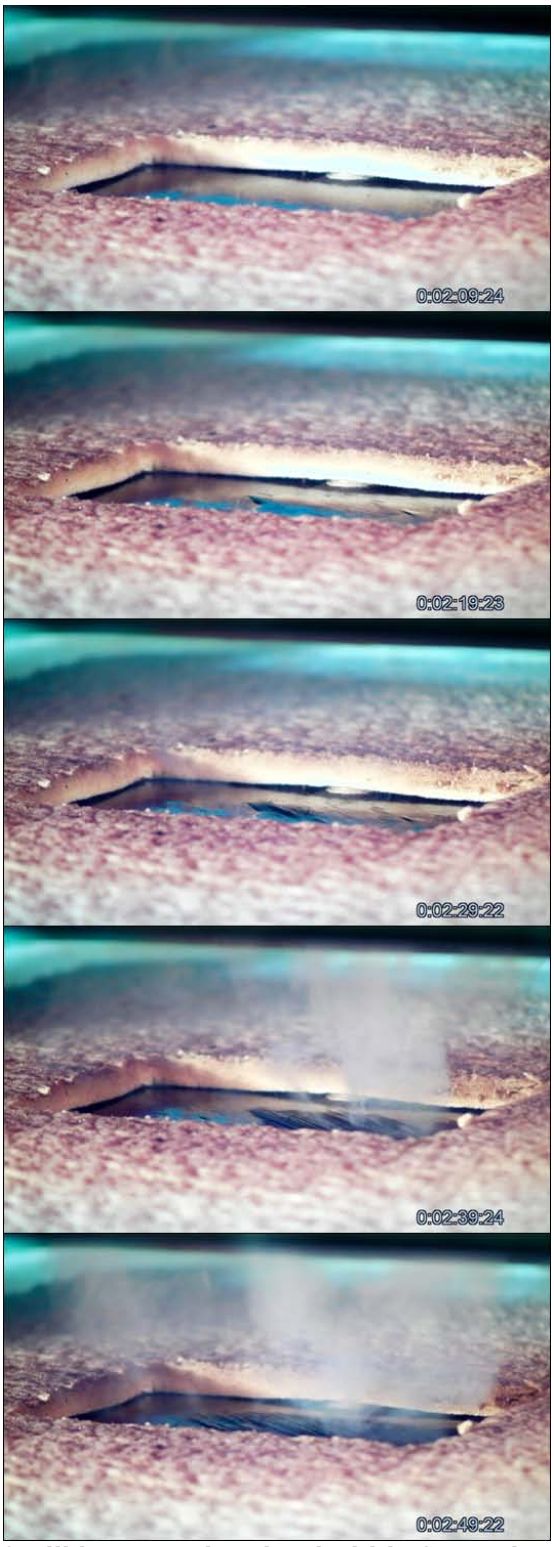

Figure 10: Time sequence of still images showing bubble formation under the top lamina, cracking, and smoke emanation from the Test 10 coupon

4.11 Hexcel Epoxy Fabric, Piloted Flame Spread (Test 11)

Temperature data presented in Appendix A, Figures A.11 through A.20 correspond to the thermocouple naming convention presented in Appendix A.11. The glow plug igniter was turned on at a coupon temperature of 300°C. Lamps remained on until the flame self-extinguished.

In test 11, smoking occurred at an elapsed time of approximately 201 seconds and was confined to a region just above the igniter (due to shielding from the igniter housing) and below the vertical midpoint of the coupon (due to the vertical irradiation gradient). Smoking was primarily in the form of jets. Flaming occurred at 258 seconds and was initially confined to the region in which smoke emanated but quickly spread across the entire coupon within 5-10 seconds. Propagation of the flame front was obscured by the presence of thick flames; quantitative description of flame spread is difficult. Flames then disappeared from the region in which smoking initially occurred. This was likely caused by char formation and is supported by photographs in Figure A.11.4(d). A phenomenon which will be called flame pulsing occurred in the upper half of the coupon. Flames oscillated three to four inches vertically along the surface with a characteristic time on the order of 0.2 seconds. The flame self-extinguished after approximately 150 seconds of flaming combustion.

Figure A.11.3(c) shows back side thermocouple measurements as differences from a reference TC (chosen as 51 mm (2”) from the bottom edge of the coupon on the insulated face). It is recommended that these back side temperature profiles be used for model development and validation along with the shroud temperature for radiative boundary conditions. The temperature differences reached a maximum near the transition to smoking and then decreased. This is potentially indicative of a change in energy transport as resin decomposition begins. Some heat transferred to the test coupon is absorbed during pyrolysis rather than causing an increase in temperature. Emission of volatile gases may also alter heat transfer to the surface through the addition of convective currents. Another inflection point appears at approximately 300 seconds after 40 seconds of flaming combustion. Temperature differences then began to rise and subsequently level off toward self-extinguishing. The temperature difference with respect to the top-front face thermocouple (T2-TFT) is negative after flaming occurred. Flames likely penetrated underneath the Zirconia board mask and affected temperature measurements. The front face-top thermocouple may therefore be a better indicator of flame temperature (630°C maximum) than surface temperature. It is for this reason, front side thermocouple measurements are not recommended for model validation.

Char formation was observed and is shown in Figure 11.4(d). This is the region in which smoking initially occurred and subsequently transitioned to flaming. Char potentially insulates the solid and limits the transport of volatile gases to the surface. This region was the first to self-extinguish, but flames persisted for a longer period in the upper half of the coupon. Pyrometer measurements are questionable and should not be used for model validation. Radiation from the shroud may have interfered with surface measurements at the beginning. Then, after the onset of flaming, the surface was obscured by flames and soot.

4.12 Hexcel Epoxy Fabric, Piloted Flame Spread (Test 12)

Test 12 displayed trends similar to those in test 11. Smoking began at an elapsed time of 178 seconds and the transition to flaming combustion occurred at 225 seconds. Flames persisted

for 188 seconds and then self-extinguished. Again, char and residue were observed in the lower half of the coupon where smoking initially occurred and flaming initiated. Flames quickly traveled up the face of the test coupon and attached to the surface. Flame pulsing occurred in the final stages of combustion near the coupon edges in the upper half of the coupon. In Figure A.12.1(c), T2-TFB became negative after the onset of flaming because flames engulfed the coupon edge nearest the front face-bottom thermocouple (TFB).

4.13 Cytec Bismaleimide Fabric, Piloted Flame Spread (Test 13)

Fundamental differences in smoke production were observed for the BMI fabric sample. Tenuous wisps of smoke emanated from the bottom edge of the coupon after an elapsed time of 221 seconds. Flames initiated at 318 seconds and were confined to a small region behind the igniter housing for approximately 15 seconds. The flame then jumped over the bottom half of the coupon and attached to the surface in the upper half. Flame pulsing did occur in the top half of the coupon. Isolated flamelets were observed on the surface. Less vigorous flames persisted for a total of 310 seconds. Residue covered the Zirconia board mask above coupon, however, no residue was found on the face of the coupon.

4.14 Cytec Bismaleimide Fabric, Piloted Flame Spread (Test 14)

Smoke production began at an elapsed time of 219 seconds and was noticeably thinner than for Hexcel epoxy fabric samples. The rate of flame spread also appeared slower and flames did not immediately attach to the upper half of the coupon. The final minutes of flaming combustion were characterized by modest flames lasting 0.1-0.2 seconds which self-extinguished and re-ignited at intervals of approximately 5 seconds. Very little residue was found on the coupon or Zirconia board mask in contrast to test 13.

4.15 Cytec Epoxy Fabric, Piloted Flame Spread (Test 15)

Heavy jet-like smoking began at approximately 183 seconds. The region from which it emanated was a visibly charred 25-50 mm (1-2”) diameter circle. Flame quickly engulfed the charred region at 263 seconds and rapidly spread (5-10 seconds) across the surface of the coupon. Again, pulsing with a characteristic time on the order of 0.2 seconds was observed where flames oscillated up and down the coupon within the upper half. Flaming combustion persisted for 163 seconds.

4.16 Cytec Epoxy Fabric, Piloted Flame Spread (Test 16)

Similar to test 15, smoking began in a localized charred region. This region grew to consume the bottom half of the coupon before ignition at 257 seconds. The flame quickly spread and attached to the upper coupon surface.

4.17 Cytec Bismaleimide Tape, Piloted Flame Spread (Test 17)

Smoking began at 161 seconds in a region where cracking appeared parallel to the fiber orientation. The smoke was noticeably thinner and wispier than smoke emanating from epoxy

fabric samples. Flames ignited at the bottom edge and then jumped to the smoking region. The flame did not immediately attach to the upper coupon surface. Flames eventually thinned out across the surface originating from cracks perpendicular to the fiber orientation. A very thin light blue flame was also observed to cover portions of the surface and pulsate. Cracking can be seen in Figure A.17.2 (c-d). Figure 11 shows a time sequence of images from Test 17 to illustrate the following observations: onset of smoking and cracking, initiation of flaming combustion, and subsequent decay to localized flamelets.

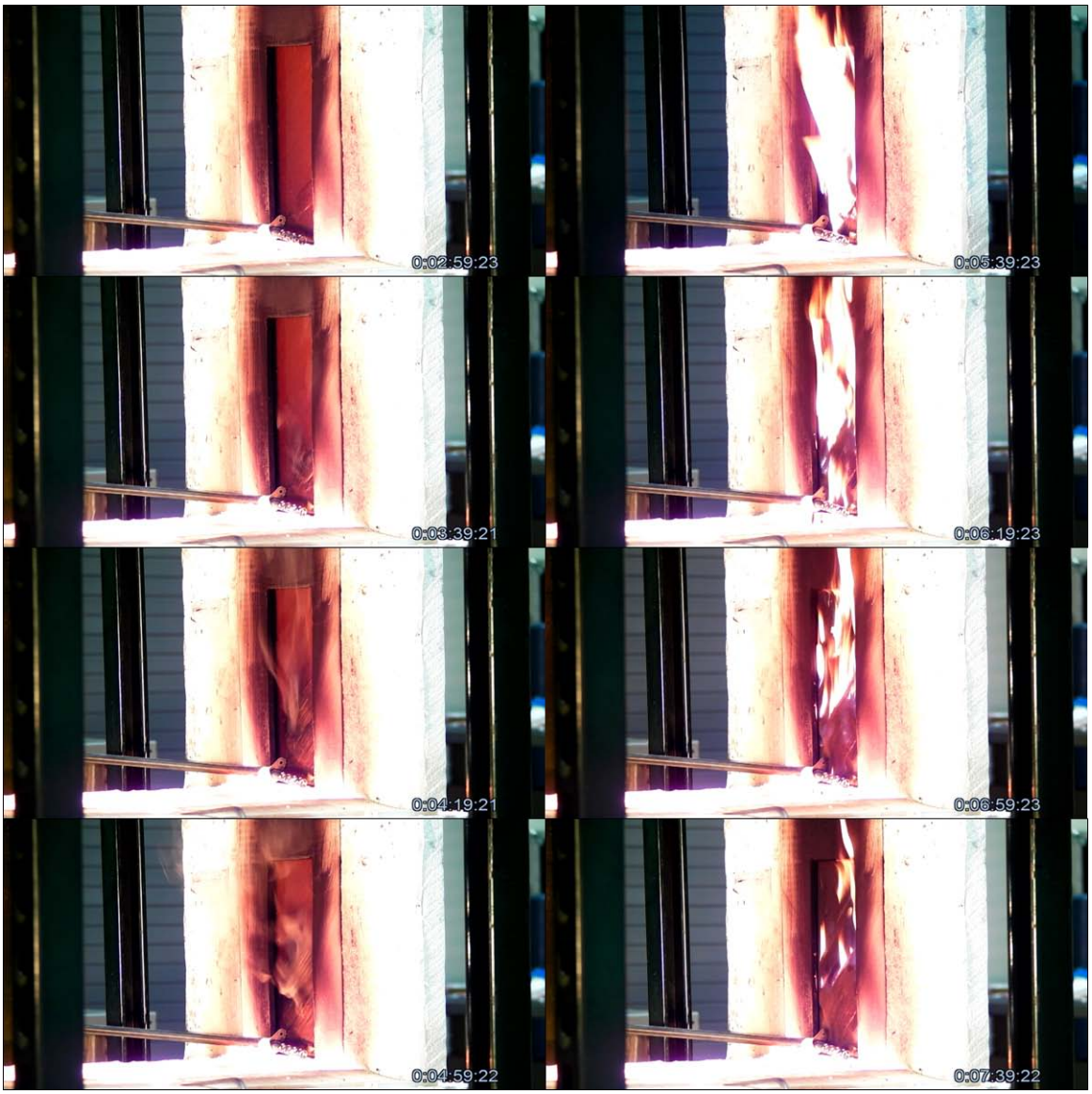

Figure 11: Time series images from Test 17 showing the onset of smoking, cracking, flaming combustion, and subsequent decay to localized flamelets

4.18 Cytec Bismaleimide Tape, Piloted Flame Spread (Test 18)

Observations from test 18 were similar to test 17.

4.19 Cytec Epoxy Tape, Piloted Flame Spread (Test 19)

Smoking began at 149 seconds and was noticeably thicker with respect to tests 17 and 18 (BMI tape). The transition to flaming occurred at 270 seconds. Smoke and flames emanated from the crack between the Zirconia board mask and surrounding fiber blanket. This could be indicative of lateral off-gassing. The flame did not propagate upward and never attached to the upper half of the coupon. Post-mortem photographs, e.g., Figure A.19.2(d), reveal a larger sub-surface layer pocket than previous tests.

4.20 Cytec Epoxy Tape, Piloted Flame Spread (Test 20)

Smoking and flaming was more vigorous than test 19. Flames propagated up the coupon and emanated from cracks. Pulsing was observed and post-mortem photographs show a sub-layer pocket similar to test 19.

5 DISCUSSION

The majority of ignition time measurements reported in the literature are piloted, e.g., cone calorimetry, and there is little available data on spontaneous combustion. The minimum reported irradiance which causes piloted ignition in glass-epoxy composites is 13 kW/m^2 (Mouritz and Gibson, 2006). Radiant heat tests conducted here were at approximately 22 kW/m^2 so it was uncertain if coupons 1-10 would ignite. The data reveal few trends that would explain why four specimens ignited and the others did not. Fan operations were varied for the tests, but since the fans are more than 20 feet above the samples and on the drawing side, the effect of the fans is thought to be small. If future tests are conducted, exhaust fan operation should be eliminated as a source of variability. Piloted ignition times show reasonable agreement with values in the literature. Bismaleimide is a high temperature thermoset resin with high thermal stability, low off-gassing, and high char yield. These characteristics result in prolonged ignition times similar to phenolic resins used in high fire risk applications. Data collected by Gibson et al. (1995) show piloted ignition for epoxy-glass fiber and phenolic-glass fiber occur at 120 seconds and 500 seconds, respectively, for an incident heat flux of 30 kW/m^2. Average ignition times measured here were 286 seconds and 247 seconds for bismaleimide and epoxy composites, respectively. The relative difference (40 seconds) does not appear statistically significant given the sample size, nor does there appear to be a significant difference between tape and fabric for a particular resin material.

The heat release rate (HRR) governs the spread of fire by providing thermal energy for growth. Flame spread and smoke generation are both functions of HRR. Char formation acts as a thermal insulator thereby preventing decomposition, and also provides additional resistance to the flow of volatile gases to the flame front. In tests 11-20, epoxy resin produced noticeably more smoke than bismaleimide although it was not quantified. This is consistent with findings of other researchers. Gibson et al. (1995) show the average smoke density for epoxy to be an order of magnitude greater than for phenolic, a material with decomposition characteristics similar to bismaleimide. Fiber orientation also affects HRR by altering the distribution of resin within the laminate. There were no noticeable differences in smoke production between tape and fabric composites. In general, smoke emanated as jets in the fabric coupons and from cracks in the tape coupons. Measurements of smoke density may be beneficial if additional tests are conducted.

Bismaleimide composites sustained flaming combustion longer than epoxy composites. Due to high char yield, one would expect these materials to self-extinguish more rapidly than epoxy. Flame intensity may explain some of this difference. Flames that persisted for a long period in BMI tests were less vigorous than those observed for epoxy materials. The material appeared to release volatile gases at a slower rate over a longer period. Little evidence of this is clearly identified in the literature.

Flame spreading rate is related to the heat release rate. The ASTM standard flame spread test (1999) measures the rate of spread down a surface at 45° decline. Measurements made with this method show downward flame front velocities of approximately 30 mm/min for epoxy-glass fiber and 0 mm/min for phenolic-glass fiber (Gibson et al., 1995). Video recordings were used to approximate flame spreading rates for epoxy coupons tested here. Flames spread approximately 152 mm (6”) over 10-20 seconds giving an estimated flame spreading rate of 380-760 mm/min. In light of this, standard methods could significantly underestimate the rate of flame spread for realistic geometries where significant portions of materials are vertical. Data

collected by Ohlemiller and Cleary (1999) show flame spreading rates, in the vertical configuration, of approximately 300 mm/min for a glass-vinyl ester composite irradiated at 11.5 kW/m^2. More work should be done to quantify the rate of flame spread from these materials. Thick flames obscured the flame front for epoxy resin composites. An inclination angle of 70-80° could be used in future tests to maintain realism while gaining better optical view of the flame front.

None of these tests exhibited surface oxidation of the char or fiber materials. Mass loss is believed to be from the composite binder only. This is presumed because there were no observed cases of partially burnt fibers, and because mass loss did not exceed the mass of the binder in the system (nominally just below 40% for the un-cured materials). Pure carbon is known to exhibit a surface oxidation type of combustion in more severe environments. Minimum temperatures for air combustion of graphitic carbon are typically found around 900º C, (see for example Babrauskas, 2003). These tests were apparently not severe enough to sustain a surface oxidation reaction, which would be evident if mass loss were higher or if fibers had severed mid-strand.

A cautionary note needs to be made here regarding this dataset. The sample composite materials we tested here are believed to be a sub-set of relevant materials to the types of fires we are considering relevant to our problems of interest. The shapes of materials we employed, however, are not believed to be highly relevant to our application space. Our dataset is expected to be valuable for model validation of simulation capabilities, but there is still need for datasets using more relevantly shaped parts. A particular concern is that the samples were small, and even though we attempted to isolate the edges from thermal effects, there is evidence presented above that suggests that a larger sample placed beneath the same exposed surface area might behave differently. The presence of fire around the edges suggests that we may be enhancing an edge effect in the burns. If we had a larger piece of material the dynamics may be different, as the gases may not be able to exit as easily along the direction of the fibers. Full delamination like that occurring in Test 4 may not be possible with larger sheets. The point of caution is that our experimental results may not be applicable to other configurations. Subsequent testing is being proposed to evaluate other shapes to obtain more relevant data.

6 REFERENCES

ASTM International. 1999. Standard Test Method for Surface Flammability of Materials Using a Radiant Heat Energy Source. ASTM E 162 – 09.

Babruskas, V., 2003. Ignition Handbook, Fire Science Publishers, Issaquah, WA, USA.

Ehlert, J.R., and T.F. Smith. 1992. View Factors for Perpendicular and Parallel Rectangular Plates. Journal of Thermophysics 7: 173-175.

Gibson, A.G., and J. Hume. 1995. Fire performance of composite panels for large marine structures. Plastics, Rubber, and Composites Processing and Applications 23: 175-183.

Mouritz, A.P., and A.G. Gibson. 2006. Fire Properties of Polymer Composite Materials. Springer, Dordrecht, The Netherlands.

Ohlemiller, T.J., and T.G. Cleary. 1999. Upward Flame Spread on Composite Materials. Fire Safety Journal 32: 159-172.

Sorathia, U. 1993. Flammability and fire safety of composite materials. In: Proceedings of the 1st International Workshop on Composite Materials for Offshore Operations. Houston, Texas, 26-28, October 1993, pp. 309-317.

Appendix A: Data, Figures, and Photographs

A.1 HEXCEL EPOXY FABRIC, RADIANT HEAT (TEST 1)

A.1.1 Photographs of Test Setup

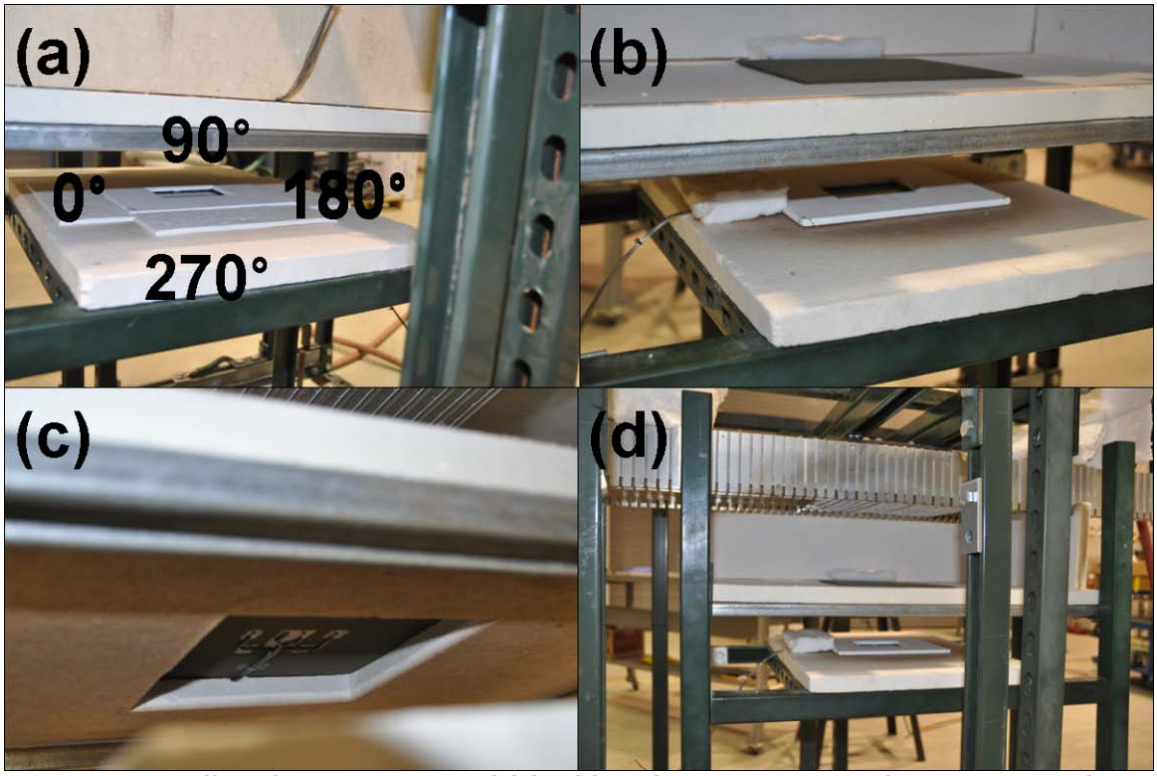

Figure A.1.1: Radiant heat test setup (a) looking down on composite coupon and mask, (b) looking down on composite coupon with top view of shroud above the coupon, (c) looking up at shroud with view of control thermocouples, and (d) looking down at coupon and mask with view of lamp array

A.1.2 Thermocouple Naming Convention

E-1	Shroud, 31.8 mm (1 ¼") off center, on "end" of shroud TC array (Fig. A.1.1(c))
E-2	Shroud, 31.8 mm (1 ¼") off center, on "end" of shroud TC array
B-Center	Composite coupon, bottom side (insulated), center
B-0	Composite coupon, bottom side (insulated), 0 degrees (Fig. A.1.1(a))
B-90	Composite coupon, bottom side (insulated), 90 degrees
B-180	Composite coupon, bottom side (insulated), 180 degrees (TC wires exit)
B-270	Composite coupon, bottom side (insulated), 270 degrees
T-0	Composite coupon, top side (irradiated), 0 degrees
T-90	Composite coupon, top side (irradiated), 90 degrees
T-180	Composite coupon, top side (irradiated), 180 degrees
T-270	Composite coupon, top side (irradiated), 270 degrees

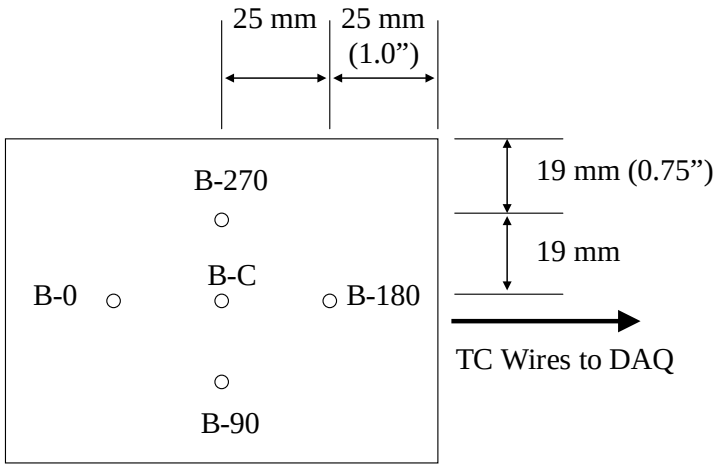

Figure A.1.2: Back side (insulated) thermocouple layout

A.1.3 Event Time Correlations

Table A.1.1: Elapsed time (seconds) from lamp ramp initialization for radiant heat tests

	Test									
Event	1	2	3	4	5	6	7	8	9	10
smoking	200	129	216	206	162	97	146	156	125	94
swelling			205	236	179	184	139	145	138	133
ignition	450	143	555						286	
lamps off	500	163	570	1557	806	833	875	962	327	643
flame extinguished	594	334	683						426	
smoking ceased		419	821	881	663	514		784		

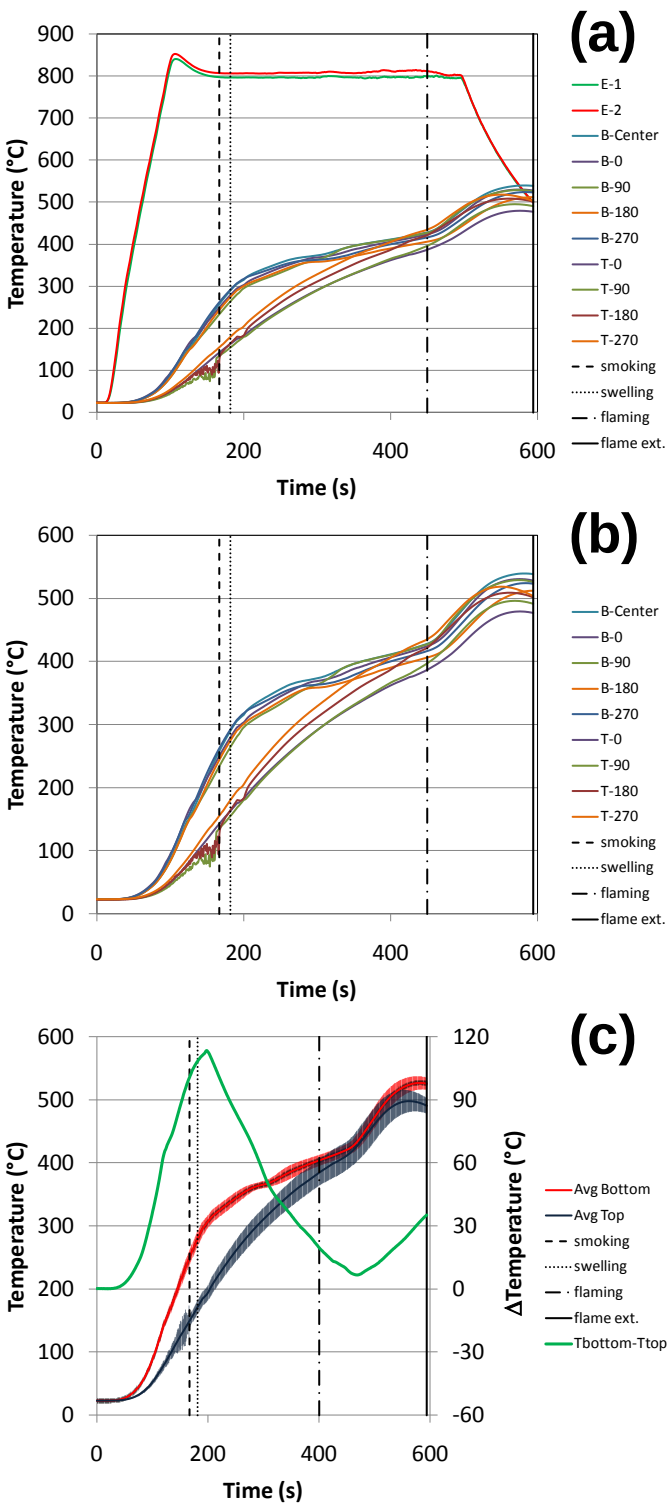

Figure A.1.3 : (a) coupon temperature and shroud temperature vs. irradiated time, (b) coupon temperature vs. irradiated time, and (c) average and standard deviation of coupon top and bottom surface temperatures, and temperature difference vs. irradiated time

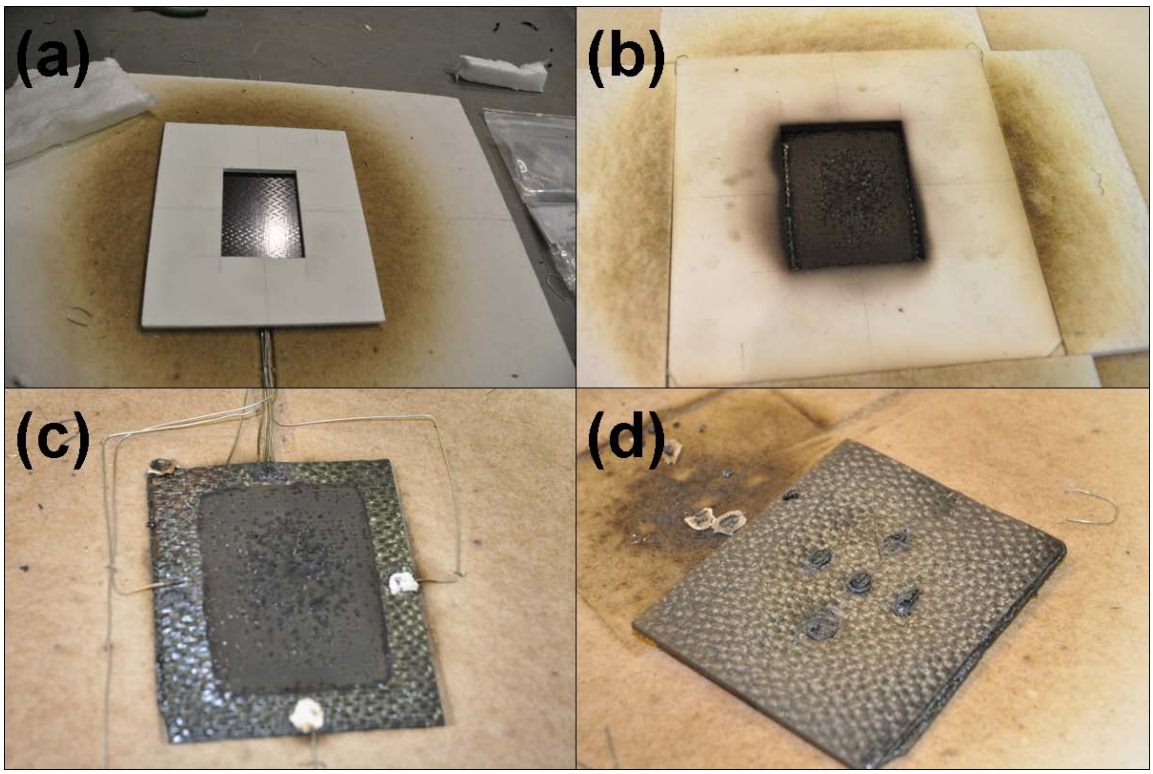

Figure A.1.4 : (a) pre-test coupon and Zirconia board mask, (b) post-test coupon and Zirconia board mask, (c) post-test top coupon face (irradiated surface), and (d) post-test bottom coupon face (insulated surface)

A.2 HEXCEL EPOXY FABRIC, RADIANT HEAT (TEST 2)

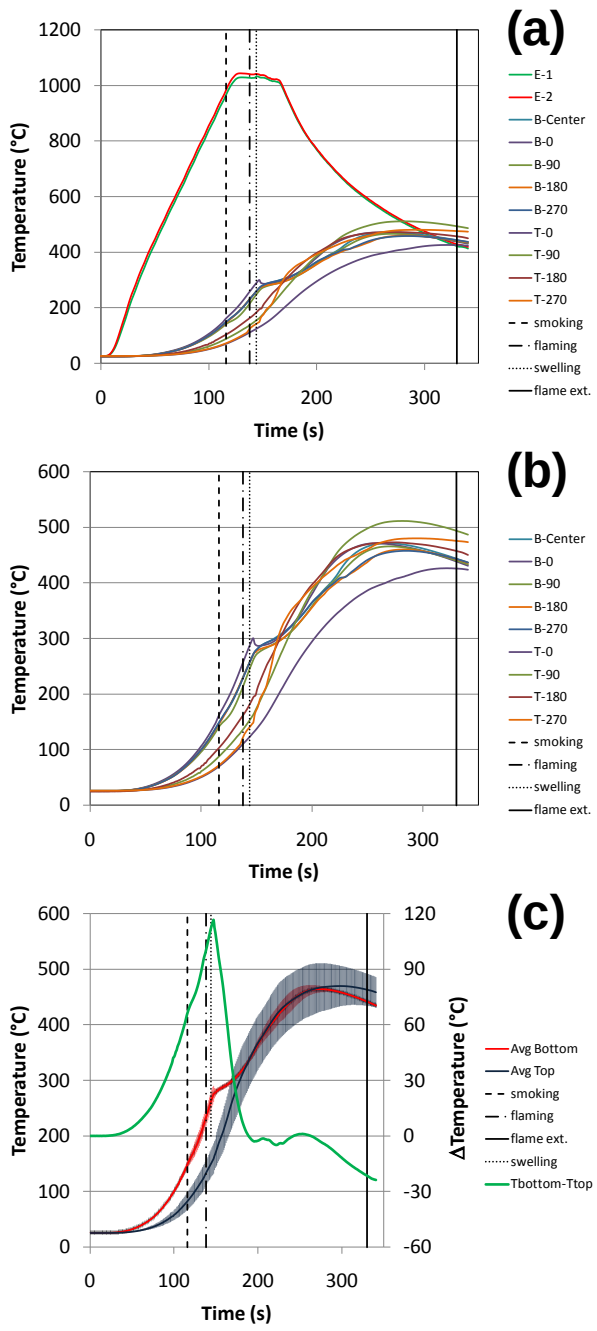

Figure A.2.1: (a) coupon temperature and shroud temperature vs. irradiated time, (b) coupon temperature vs. irradiated time, and (c) average and standard deviation of coupon top and bottom surface temperatures, and temperature difference vs. irradiated time

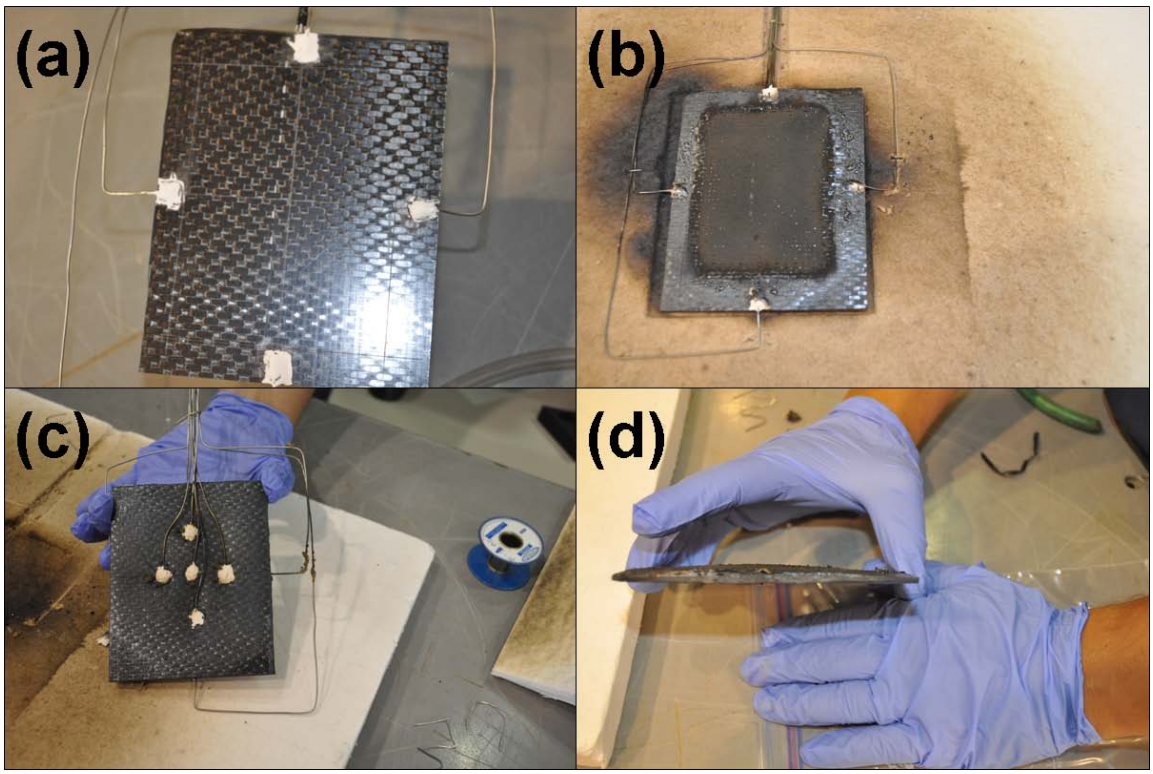

Figure A.2.2: (a) pre-test top coupon face (irradiated surface), (b) post-test top coupon face, (c) post-test bottom coupon face (insulated surface), and (d) post-test side-view of coupon

A.3 CYTEC BISMALEIMIDE FABRIC, RADIANT HEAT (TEST 3)

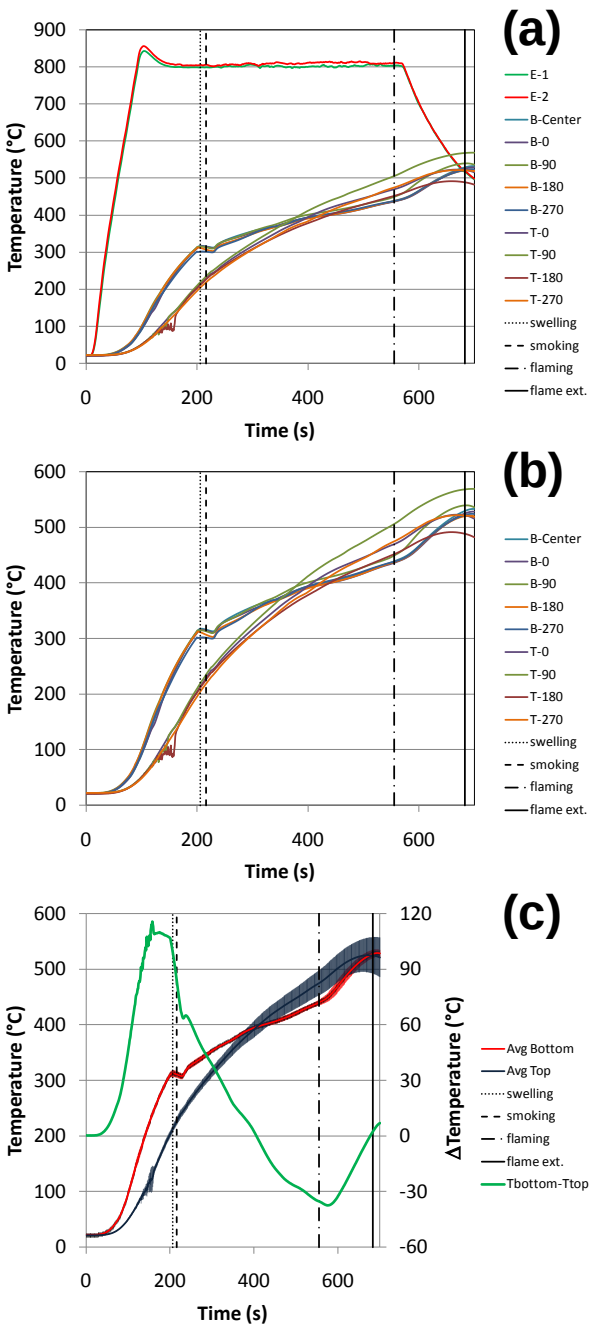

Figure A.3.1: (a) coupon temperature and shroud temperature vs. irradiated time, (b) coupon temperature vs. irradiated time, and (c) average and standard deviation of coupon top and bottom surface temperatures, and temperature difference vs. irradiated time

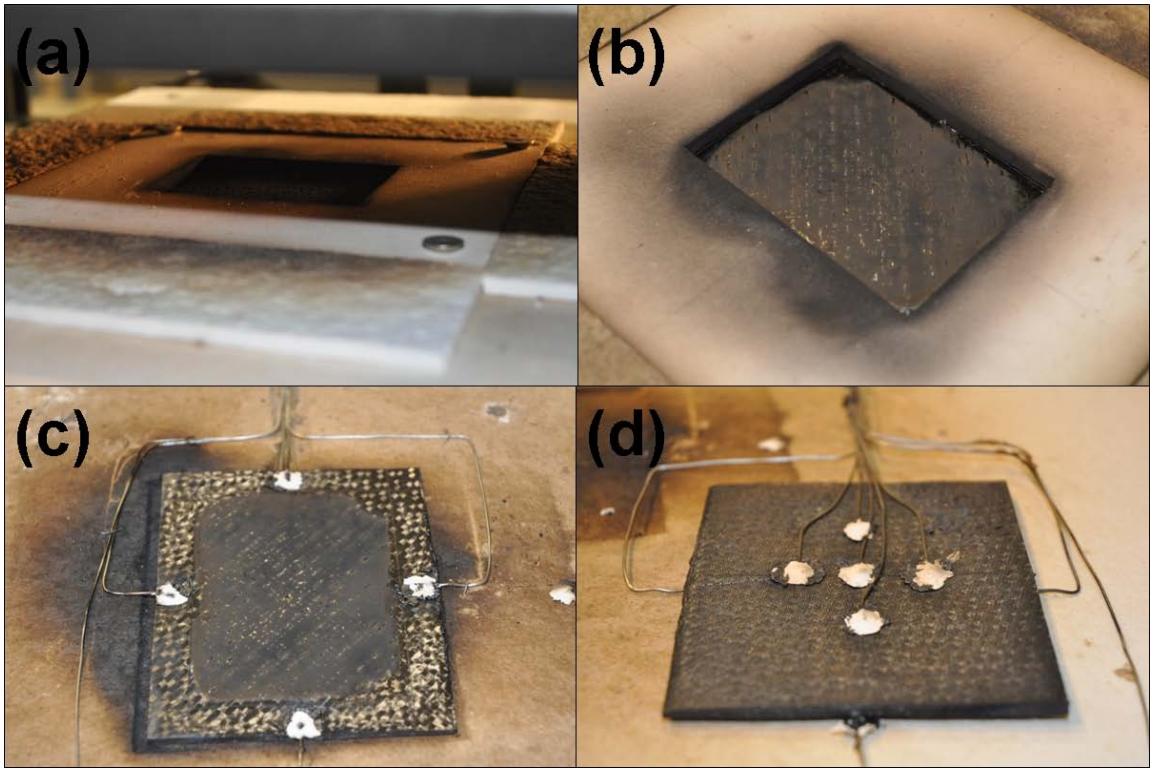

Figure A.3.2: (a) pre-test coupon in radiant heat test apparatus, (b) post-test top coupon face and Zirconia board mask, (c) post-test top coupon face (irradiated) surface), and (d) post-test bottom coupon face (insulated)

A.4 CYTEC BISMALEIMIDE FABRIC, RADIANT HEAT (TEST 4)

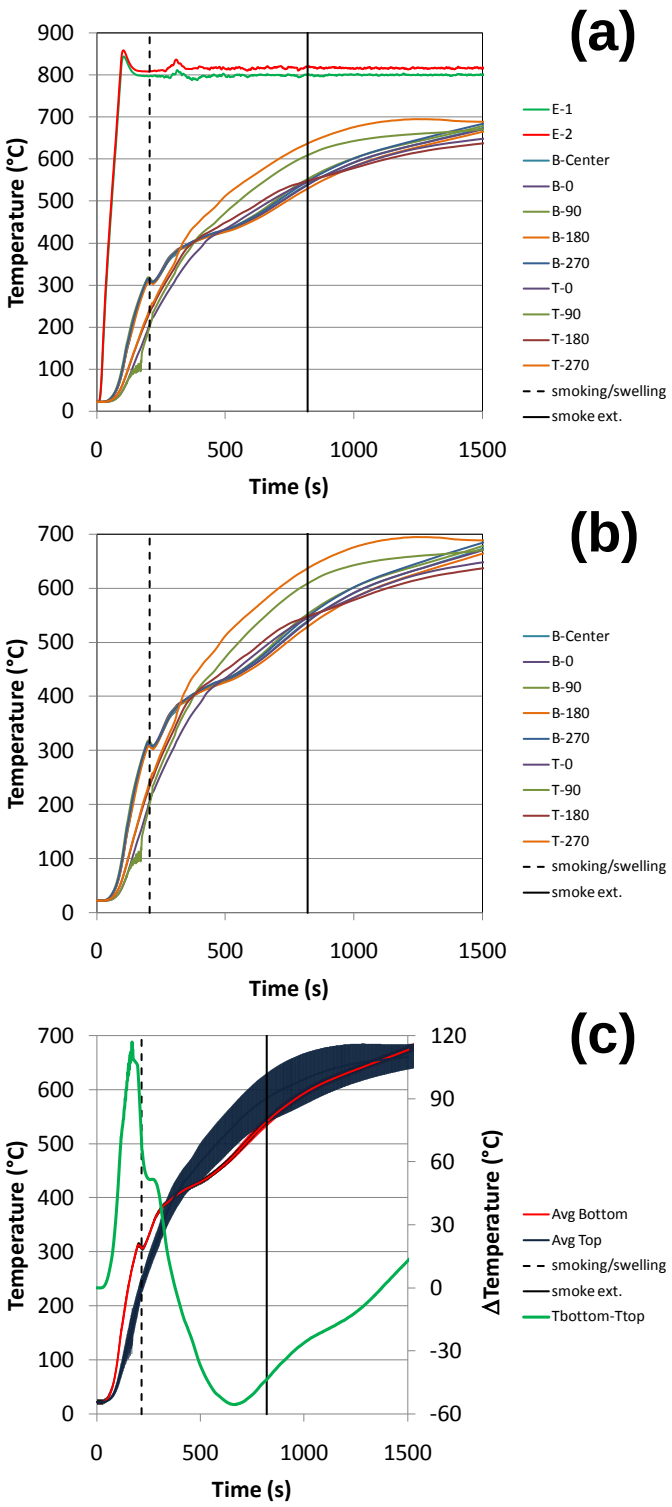

Figure A.4.1: (a) coupon temperature and shroud temperature vs. irradiated time, (b) coupon temperature vs. irradiated time, and (c) average and standard deviation of coupon top and bottom surface temperatures, and temperature difference vs. irradiated time

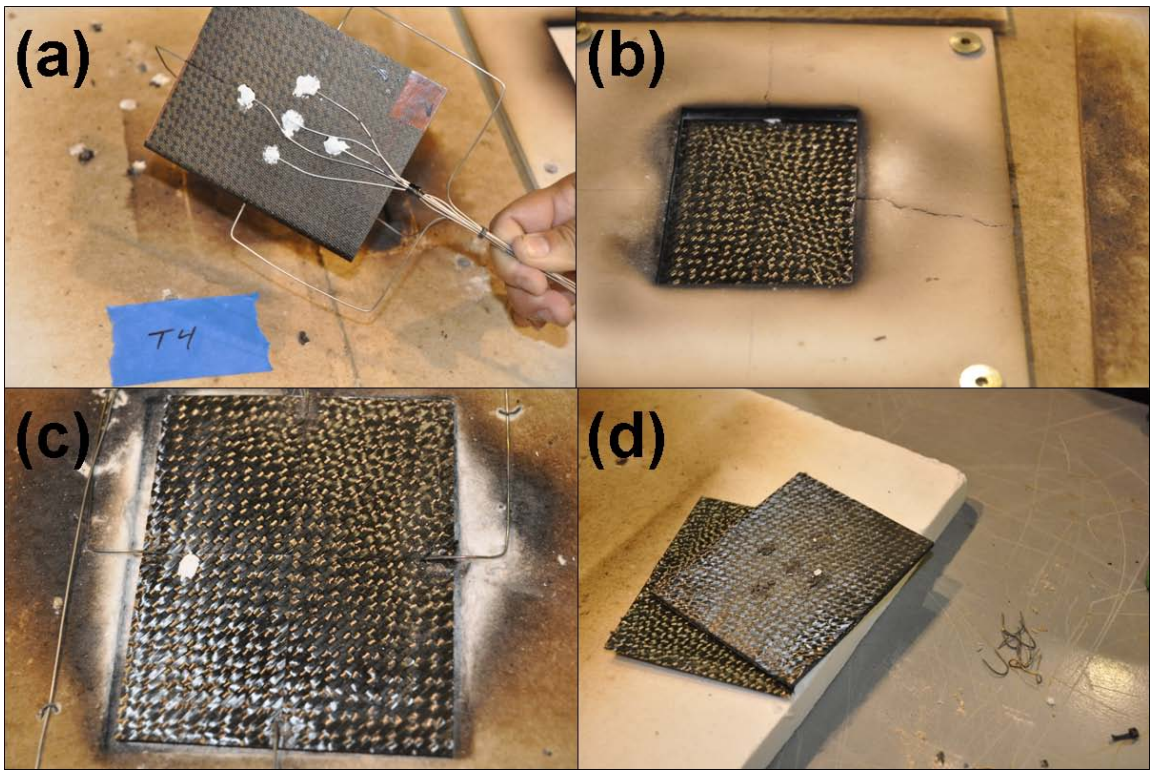

Figure A.4.2: (a) pre-test bottom coupon face, (b) post-test top coupon face and Zirconia board mask, (c) post-test top coupon face (irradiated) surface, and (d) post-test bottom coupon face (insulated) showing delamination of the top coupon layer

A.5 CYTEC EPOXY FABRIC, RADIANT HEAT (TEST 5)

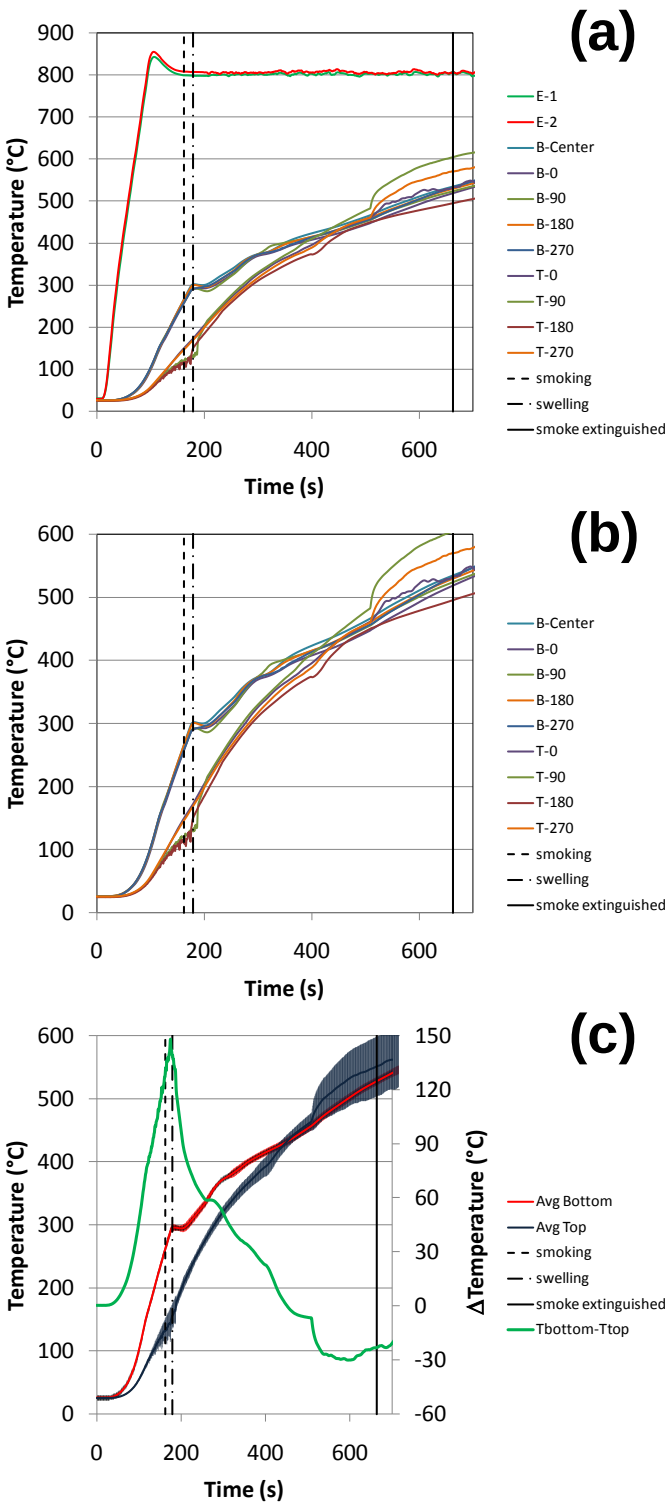

Figure A.5.1: (a) coupon temperature and shroud temperature vs. irradiated time, (b) coupon temperature vs. irradiated time, and (c) average and standard deviation of coupon top and bottom surface temperatures, and temperature difference vs. irradiated time

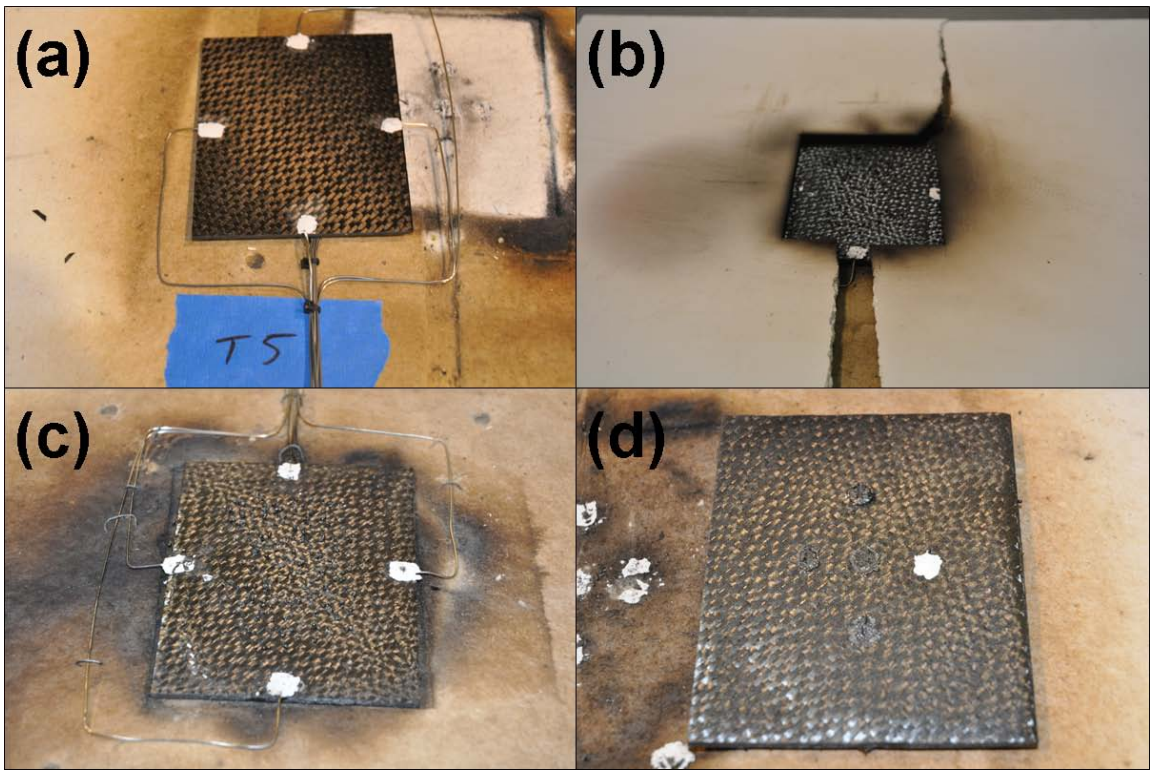

Figure A.5.2: (a) pre-test top coupon face, (b) post-test top coupon face and Zirconia board mask, (c) post-test top coupon face (irradiated) surface, and (d) post-test bottom coupon face (insulated)

A.6 CYTEC EPOXY FABRIC, RADIANT HEAT (TEST 6)

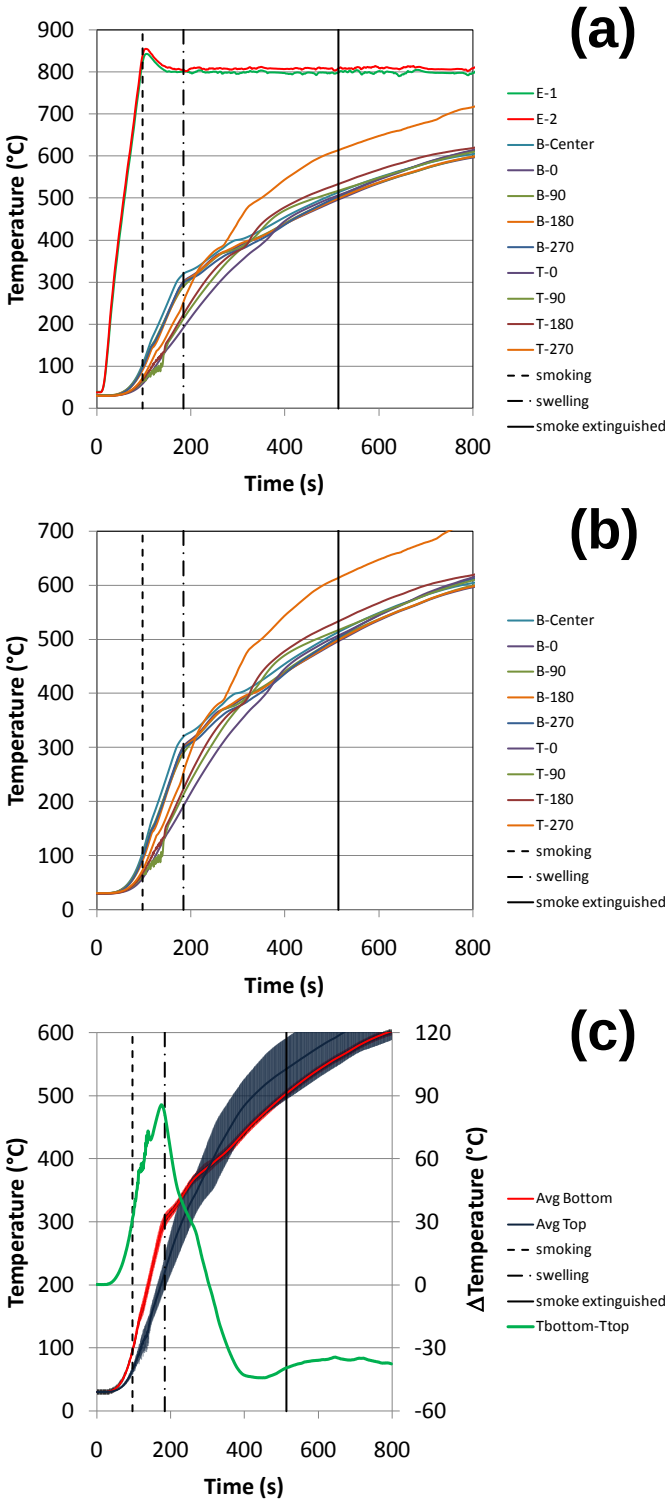

Figure A.6.1: (a) coupon temperature and shroud temperature vs. irradiated time, (b) coupon temperature vs. irradiated time, and (c) average and standard deviation of coupon top and bottom surface temperatures, and temperature difference vs. irradiated time

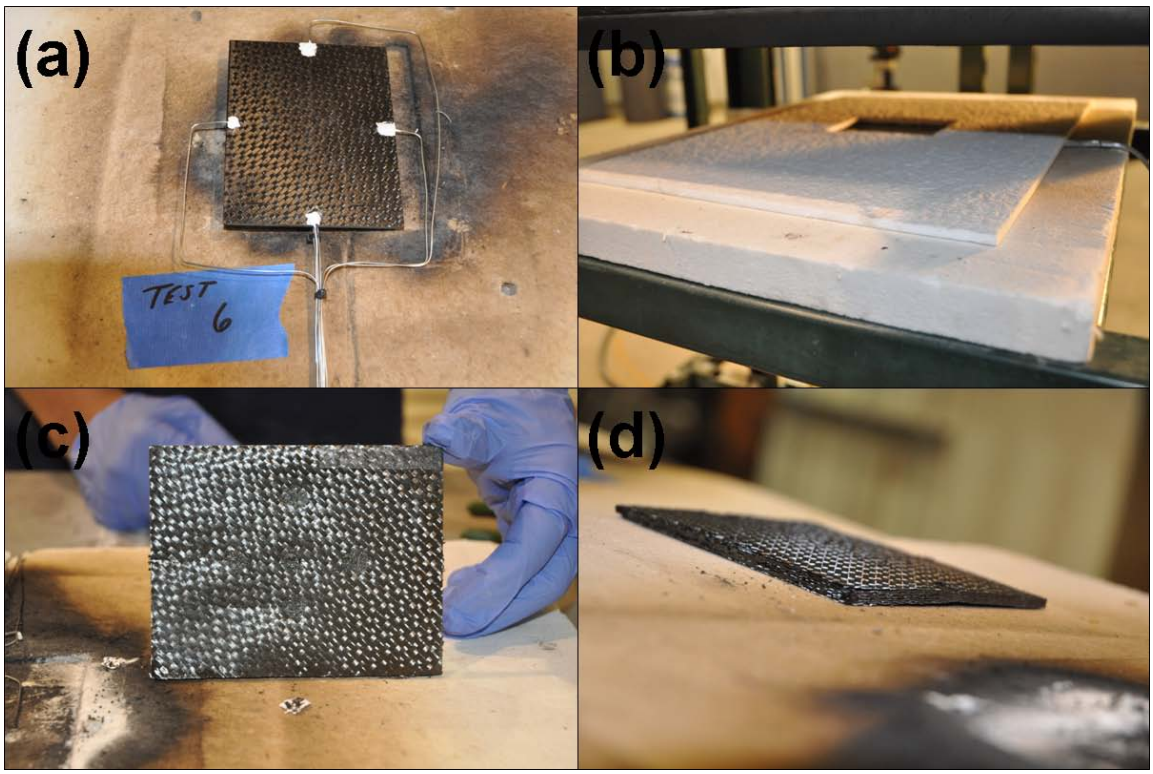

Figure A.6.2: (a) pre-test top coupon face, (b) pre-test top coupon face and fiber blanket mask, (c) post-test bottom coupon face (insulated) surface, and (d) post-test side-view of coupon showing significant volumetric expansion

A.7 CYTEC BISMALEIMIDE TAPE, RADIANT HEAT (TEST 7)

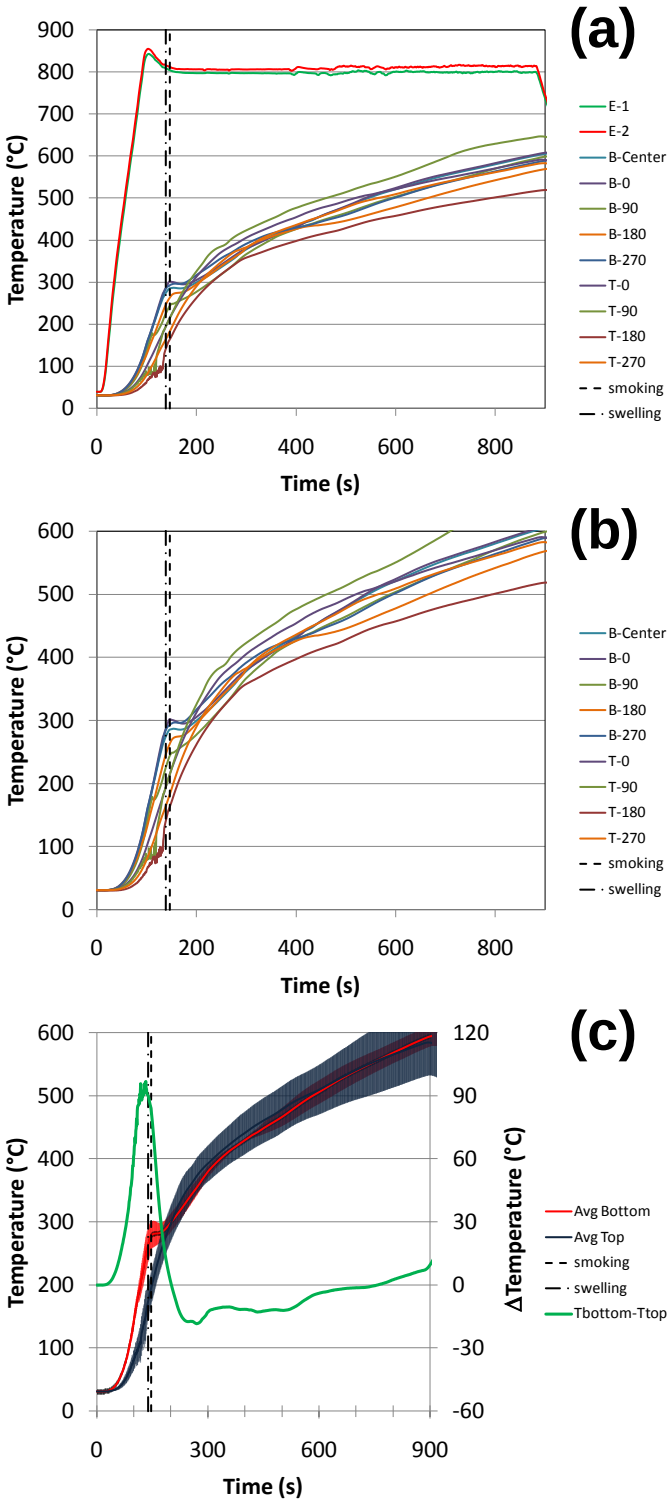

Figure A.7.1: (a) coupon temperature and shroud temperature vs. irradiated time, (b) coupon temperature vs. irradiated time, and (c) average and standard deviation of coupon top and bottom surface temperatures, and temperature difference vs. irradiated time

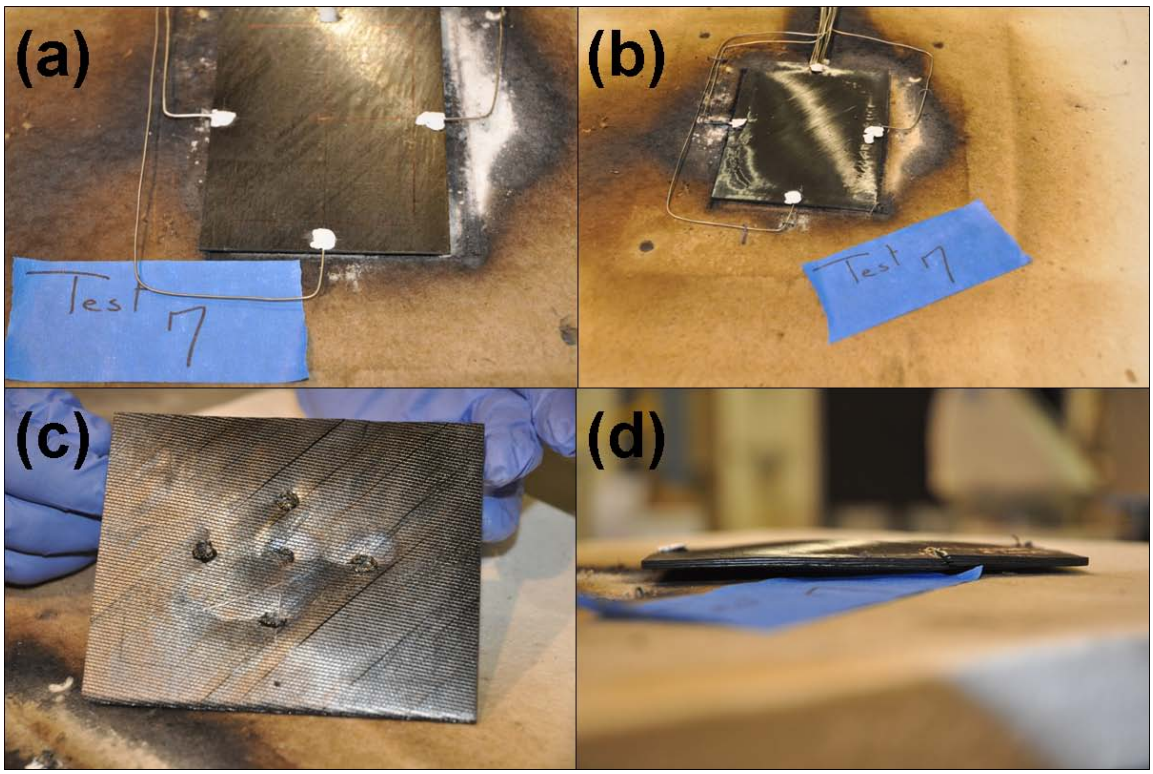

Figure A.7.2: (a) pre-test top coupon face, (b) post-test top coupon face, (c) post-test bottom coupon face (irradiated) surface, showing cracking parallel to the direction of carbon fibers, and (d) post-test side-view showing delamination throughout the coupon thickness

A.8 CYTEC BISMALEIMIDE TAPE, RADIANT HEAT (TEST 8)

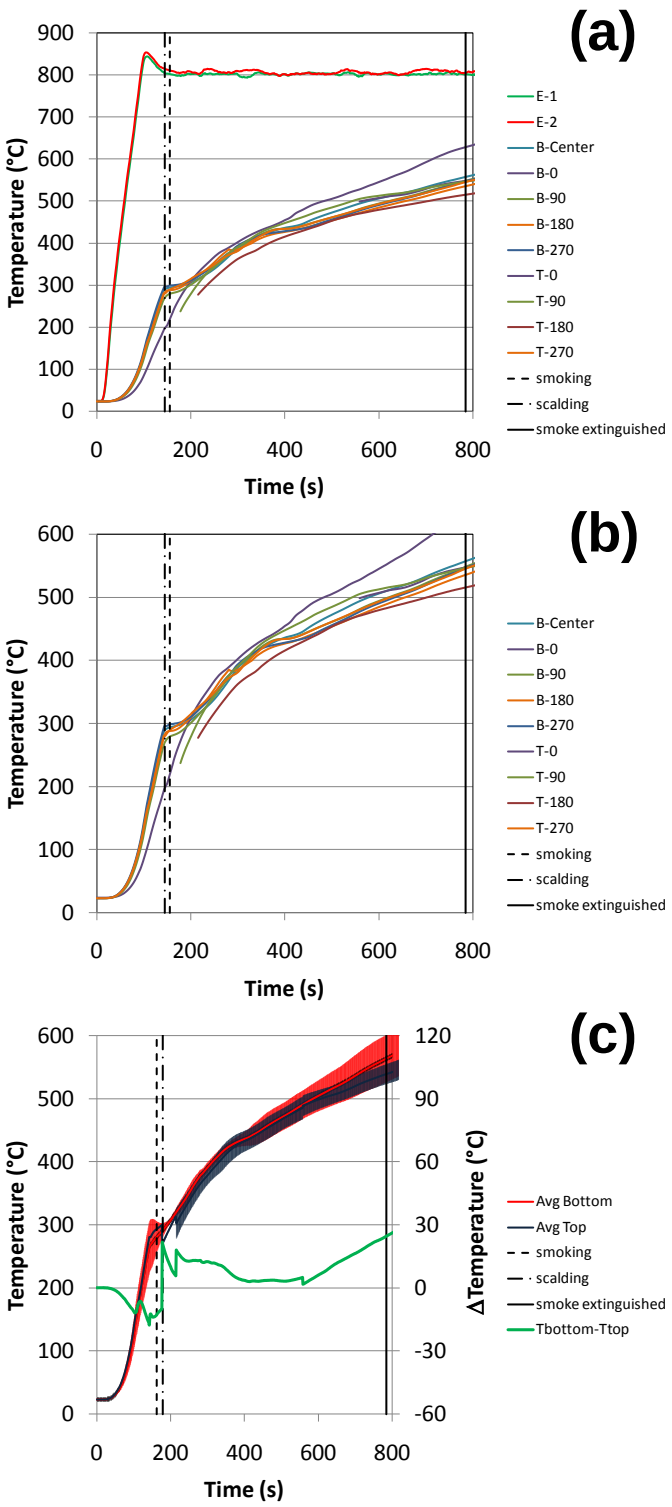

Figure A.8.1: (a) coupon temperature and shroud temperature vs. irradiated time, (b) coupon temperature vs. irradiated time, and (c) average and standard deviation of coupon top and bottom surface temperatures, and temperature difference vs. irradiated time

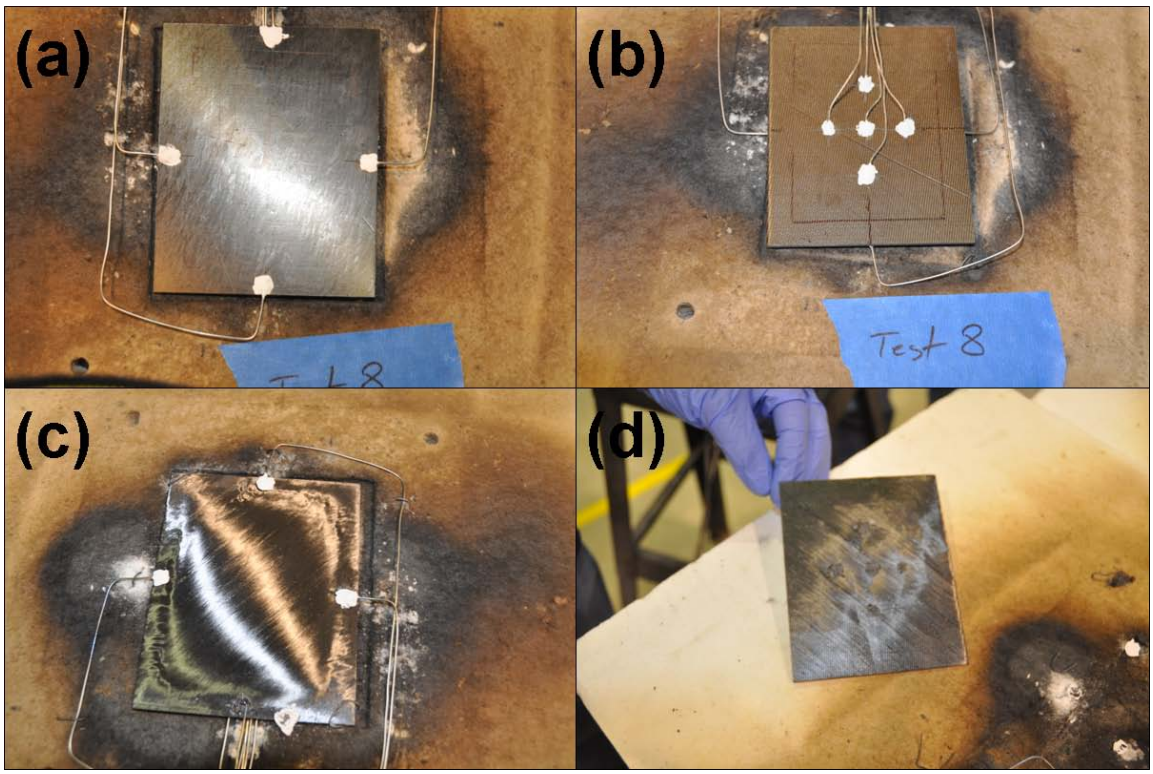

Figure A.8.2: (a) pre-test top coupon face, (b) pre-test bottom coupon face, (c) post-test top coupon face (irradiated) surface, and (d) post-test bottom coupon face

A.9 CYTEC EPOXY TAPE, RADIANT HEAT (TEST 9)

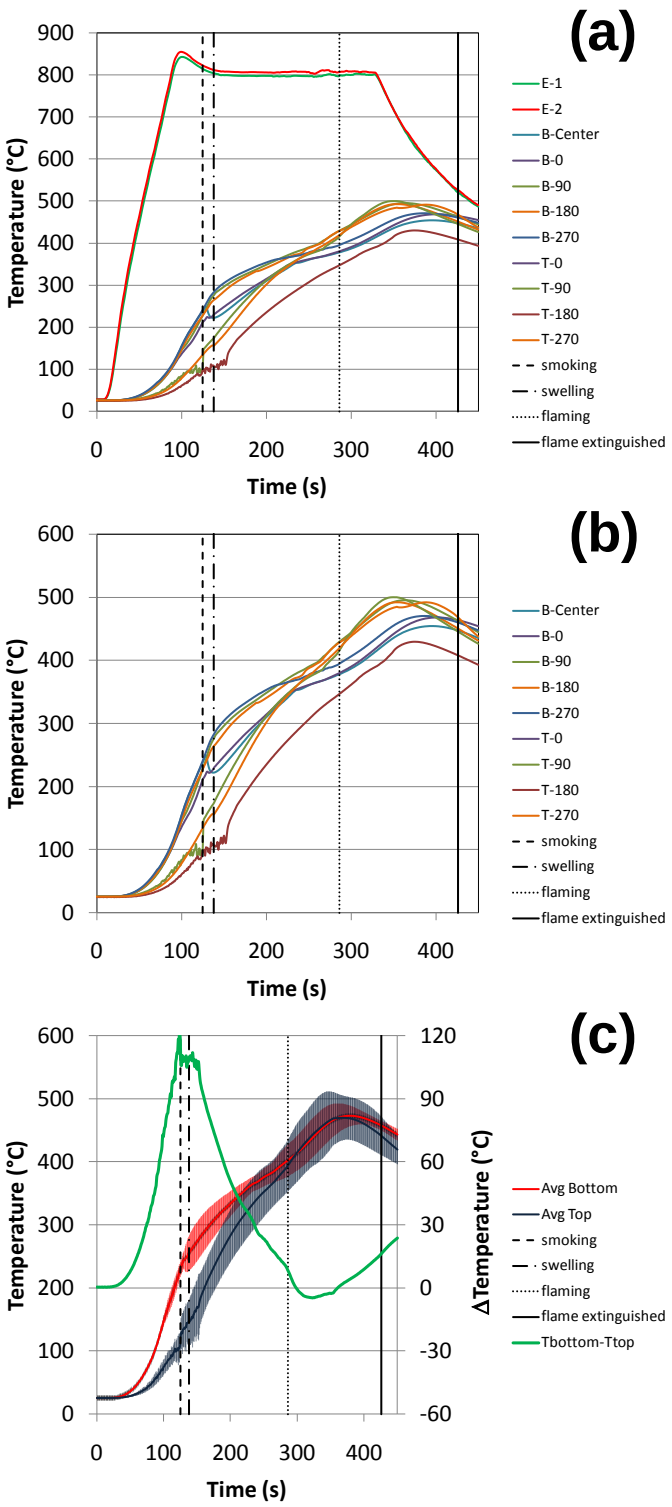

Figure A.9.1: (a) coupon temperature and shroud temperature vs. irradiated time, (b) coupon temperature vs. irradiated time, and (c) average and standard deviation of coupon top and bottom surface temperatures, and temperature difference vs. irradiated time

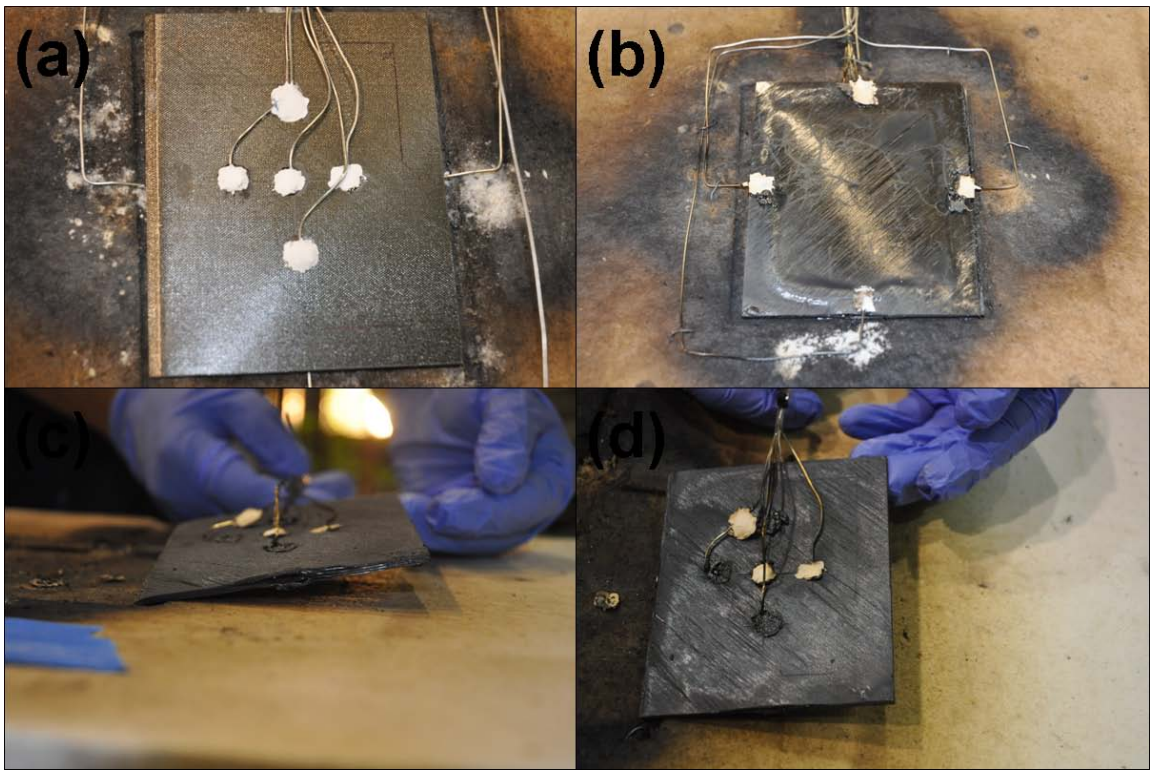

Figure A.9.2: (a) pre-test bottom coupon face, (b) post-test top coupon face showing cracking, (c) post-test coupon side-view showing significant delamination and expansion, and (d) post-test bottom coupon face showing cracks parallel to the carbon fiber direction

A.10 CYTEC EPOXY TAPE, RADIANT HEAT (TEST 10)

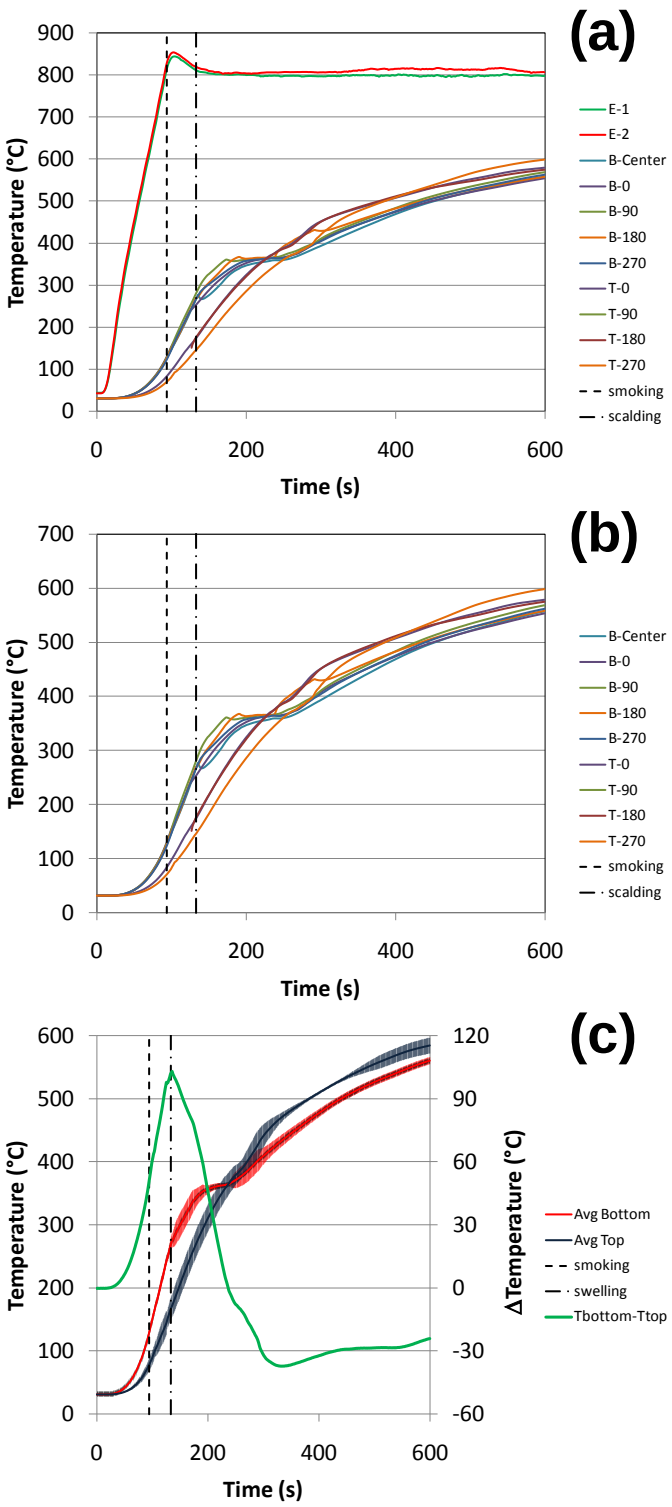

Figure A.10.1: (a) coupon temperature and shroud temperature vs. irradiated time, (b) coupon temperature vs. irradiated time, and (c) average and standard deviation of coupon top and bottom surface temperatures, and temperature difference vs. irradiated time

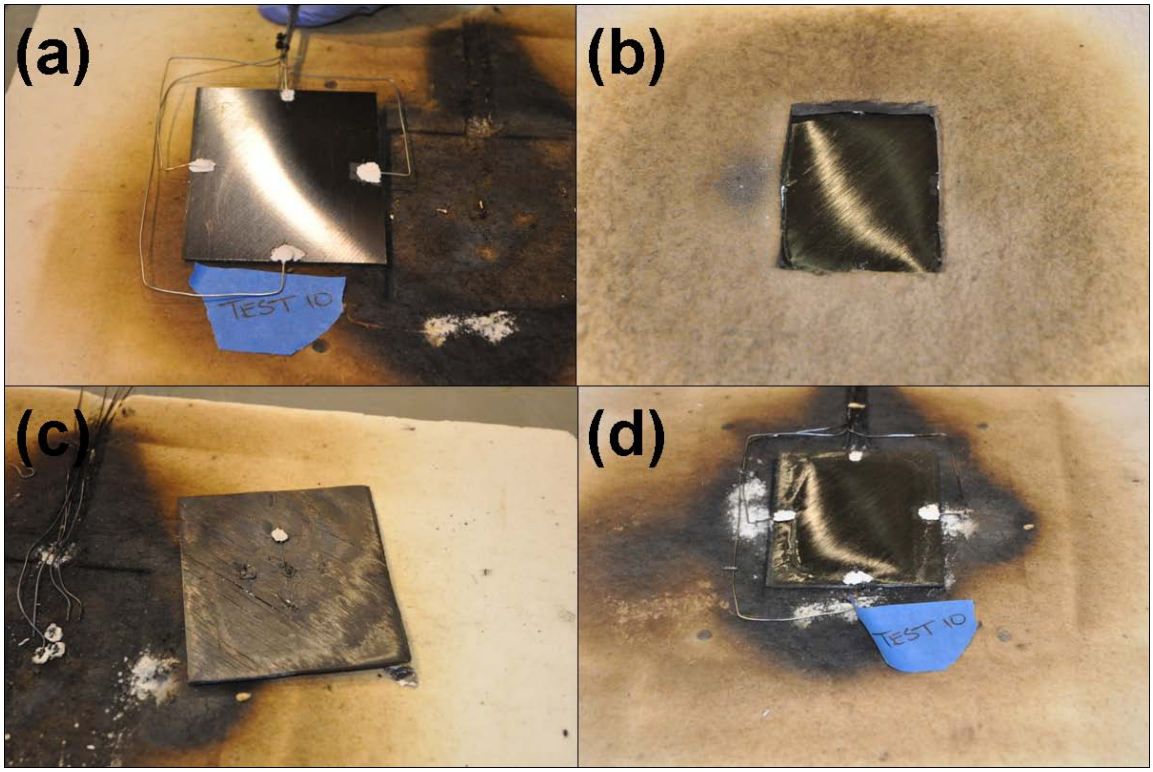

Figure A.10.2: (a) pre-test top coupon face, (b) post-test top coupon face and fiber blanket mask, (c) post-test bottom coupon face, and (d) post-test top coupon face

A.11 HEXCEL EPOXY FABRIC, PILOTED FLAME SPREAD (TEST 11)

A.11.1 Photographs of Test Setup

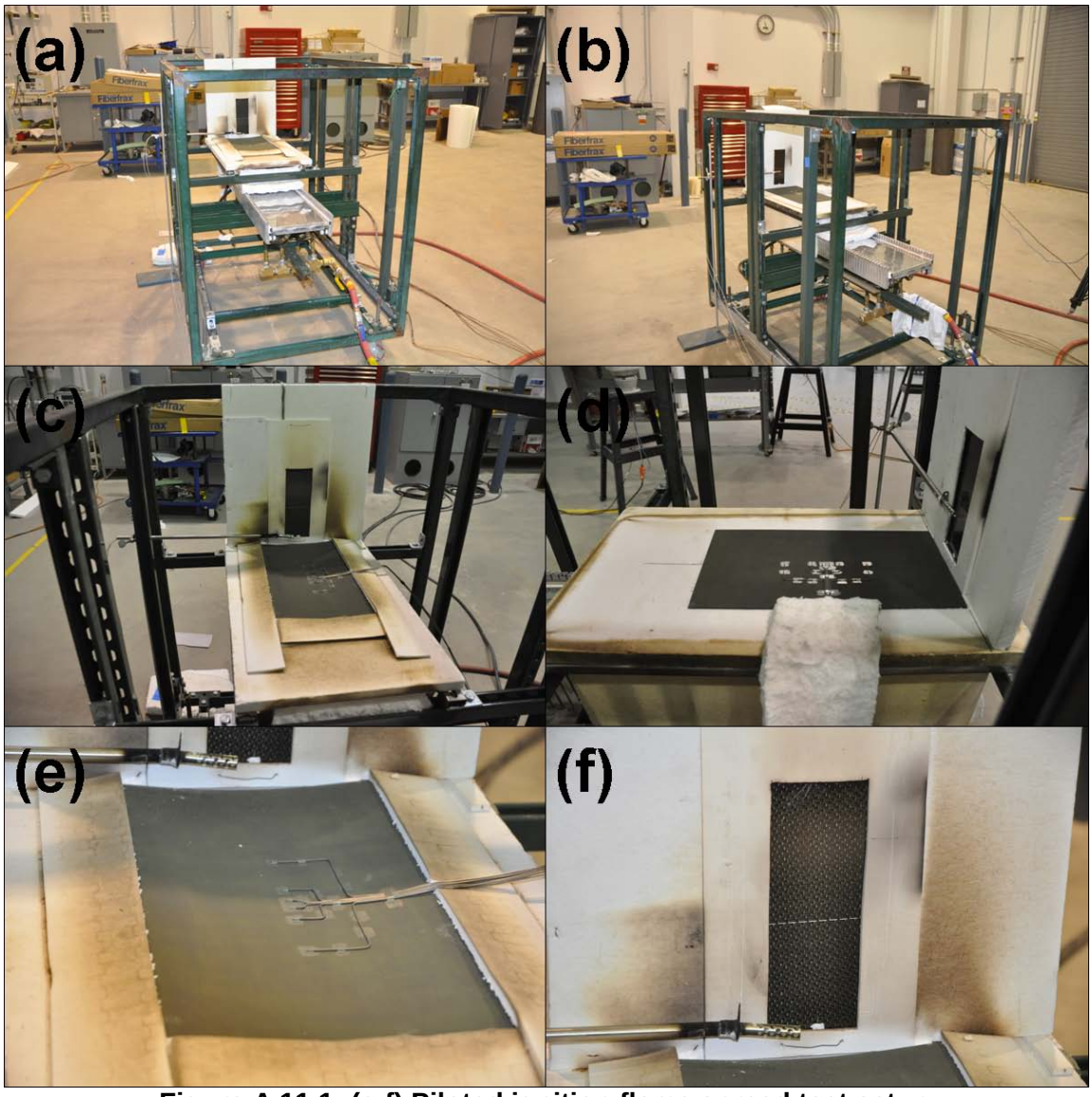

Figure A.11.1: (a-f) Piloted ignition flame spread test setup

A.11.2 Thermocouple Naming Convention

S-1E	Shroud temperature at location 1 (76 mm (3”) off center, furthest from composite coupon)
S-2	Shroud temperature at location 2 (25 mm (1”) off center, furthest from composite coupon)
S-5	Shroud temperature at location 5 (25 mm (1”) off center, closest to composite coupon)
S-6	Shroud temperature at location 6 (76 mm (3”) off center, closest to composite coupon)
2	Composite coupon, back side (insulated), 51 mm (2”) above bottom edge of coupon
3.5	Composite coupon, back side (insulated), 89 mm (3.5”) above bottom edge of coupon
5	Composite coupon, back side (insulated), 127 mm (5”) above bottom edge of coupon
6.5	Composite coupon, back side (insulated), 165 mm (6.5”) above bottom edge of coupon
8	Composite coupon, back side (insulated), 203 mm (8”) above bottom edge of coupon
F-B	Composite coupon, front side (irradiated), bottom (6 mm (1/4”) below bottom edge of mask)
F-T	Composite coupon, front side (irradiated), top (6 mm (1/4”) above top edge of mask)

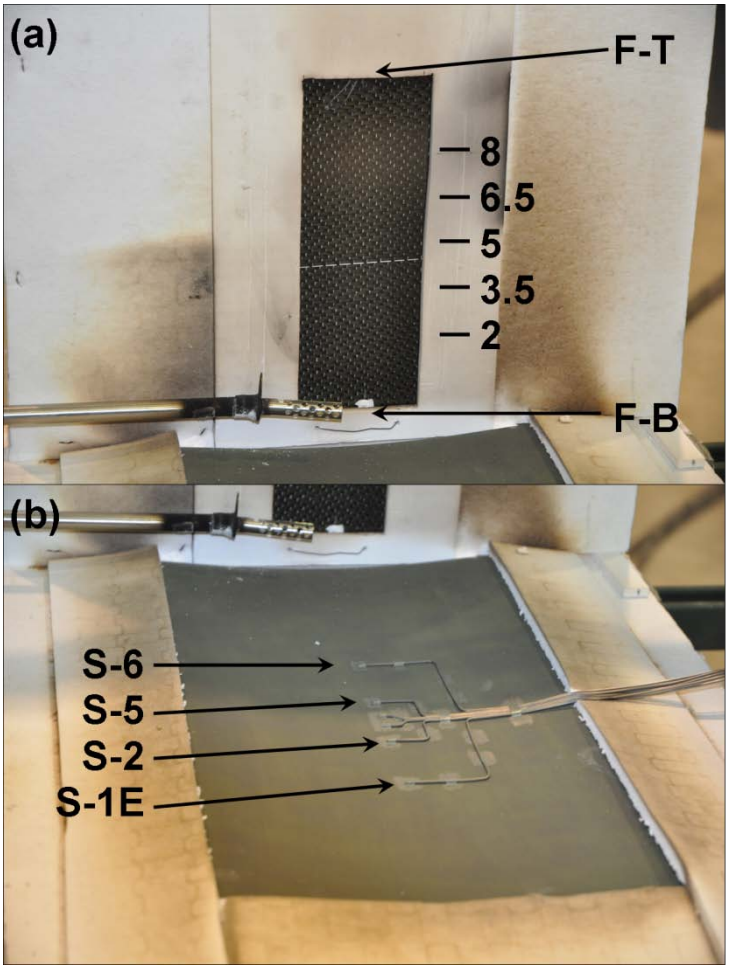

Figure A.11.2: Thermocouple layout and naming convention for piloted ignition tests (a) composite coupon, and (b) Inconel 600 shroud

A.11.3 Event Time Correlations

Table A.11.1: Elapsed time (seconds) from lamp ramp initialization for piloted ignition flame spread tests

	Test									
Event	11	12	13	14	15	16	17	18	19	20
Smoking	201	178	221	219	183	176	161	156	149	155
Ignition	258	225	319	249	263	257	303	272	270	198
flame extinguished	408	413	629	510	426	389	490	554	379	320

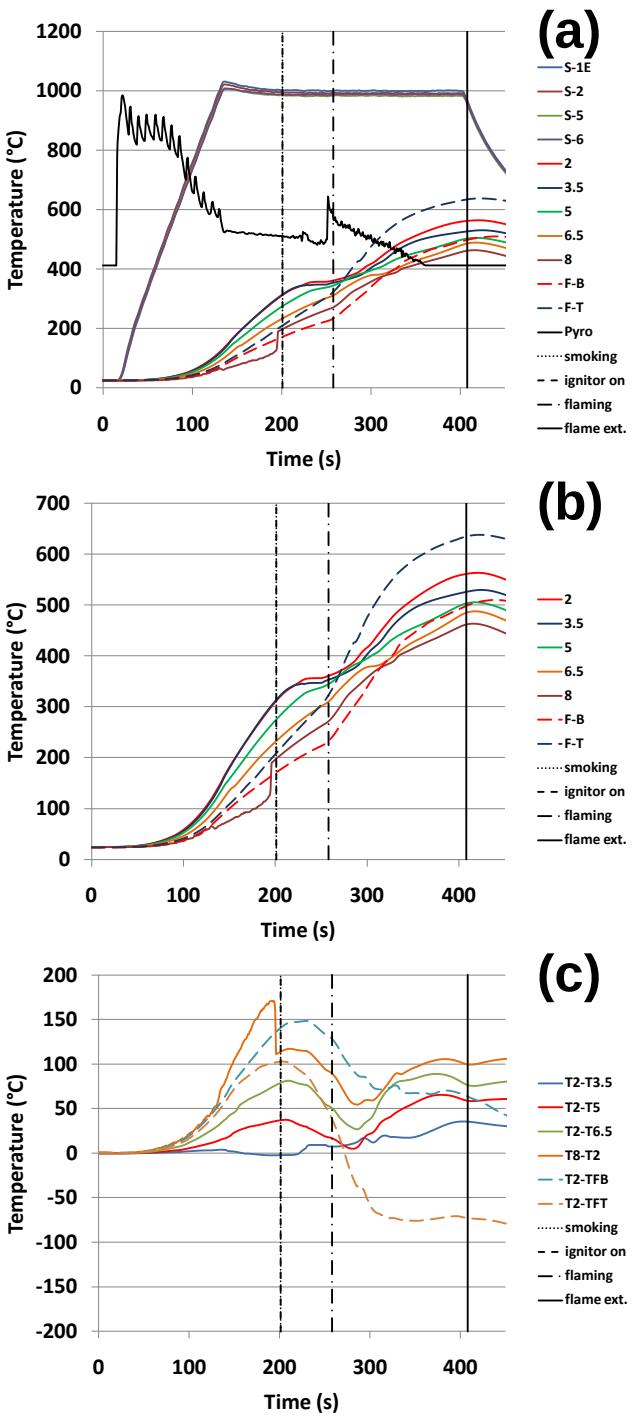

Figure A.11.3: (a) Shroud, pyrometer, and composite coupon temperature (°C) vs. elapsed time (s), (b) composite coupon temperature vs. elapsed time, and (c) composite coupon temperature differences (°C) with respect to thermocouple T2 (insulated side of coupon, 2 inches from bottom)

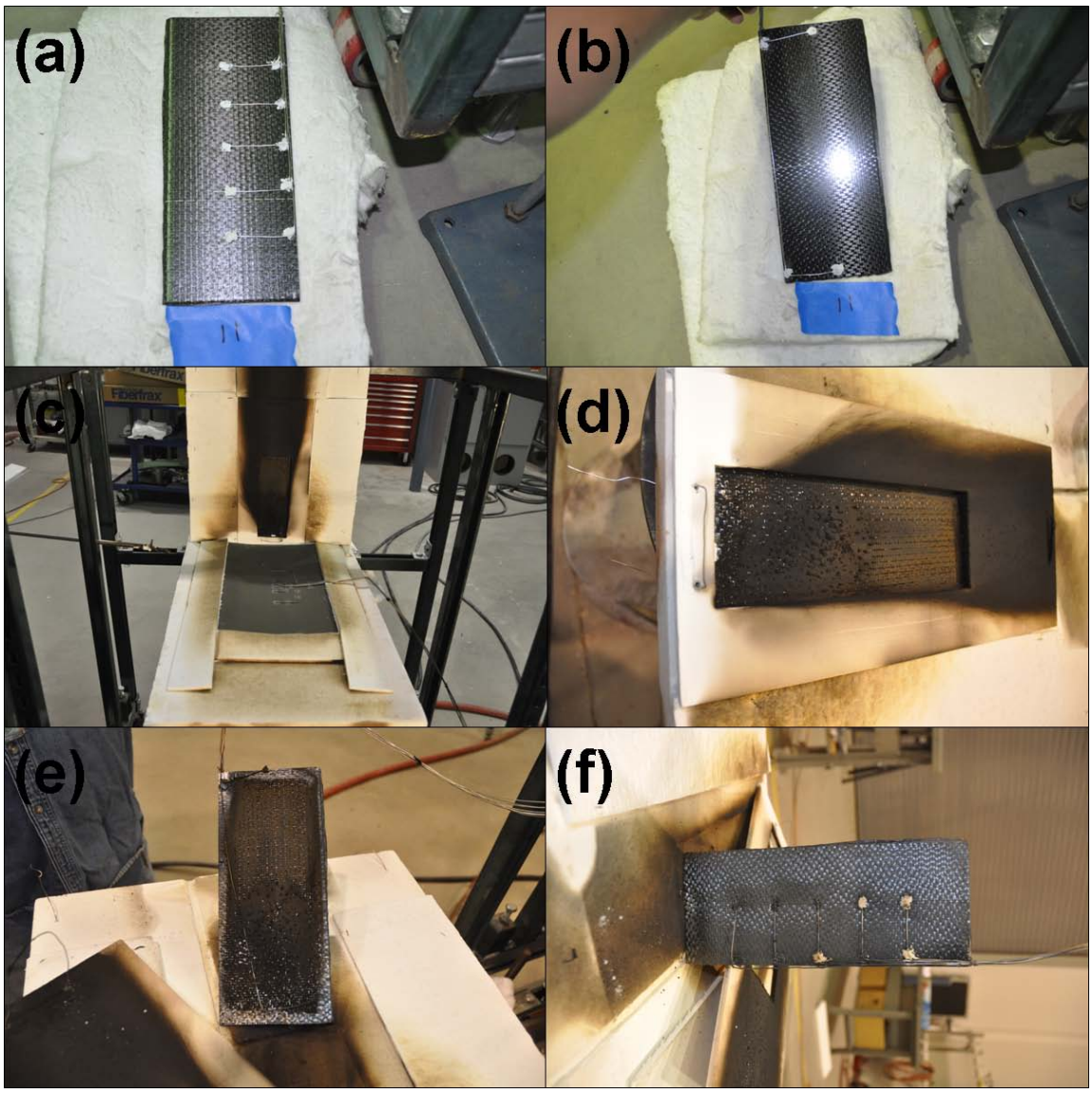

Figure A.11.4: (a) pre-test, coupon back side (insulated), (b) pre-test, coupon front side (irradiated), (c) pre-test setup, (d) post-test coupon front side, (e) post-test coupon front side, and (f) post-test coupon back side

A.12 HEXCEL EPOXY FABRIC, PILOTED FLAME SPREAD (TEST 12)

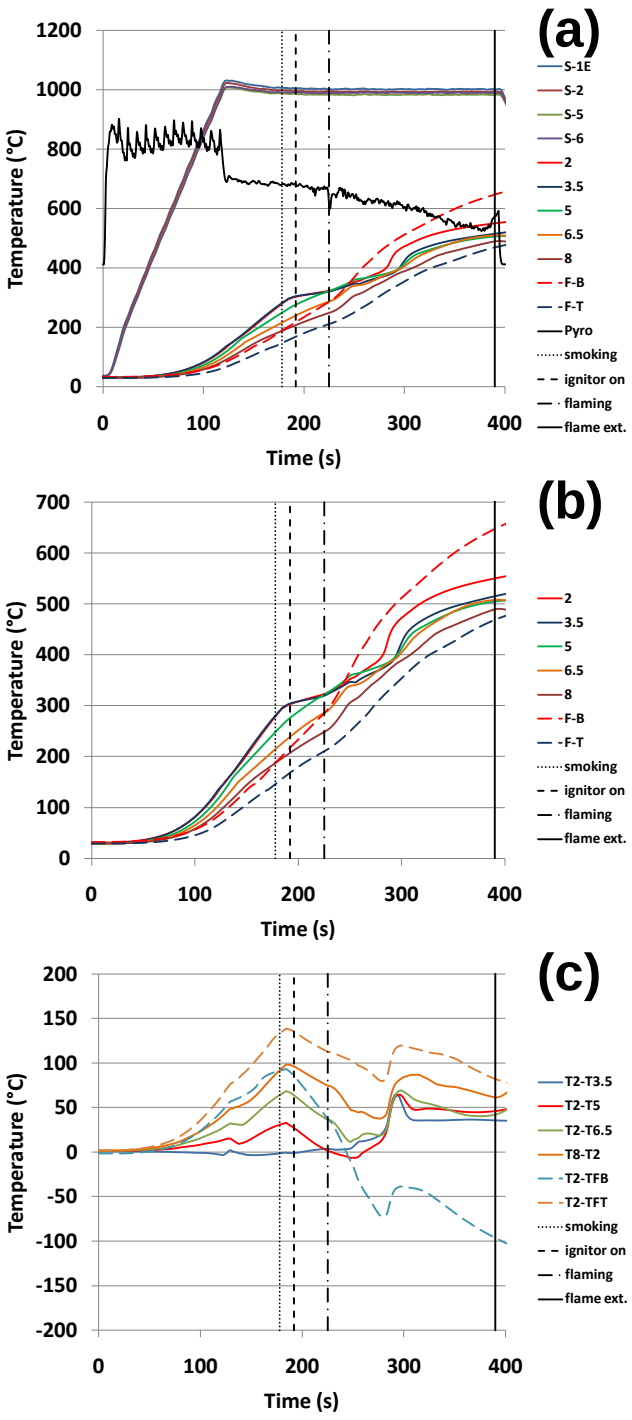

Figure A.12.1: (a) Shroud, pyrometer, and composite coupon temperature (°C) vs. elapsed time (s), (b) composite coupon temperature vs. elapsed time, and (c) composite coupon temperature differences (°C) with respect to thermocouple T2 (insulated side of coupon, 2 inches from bottom)

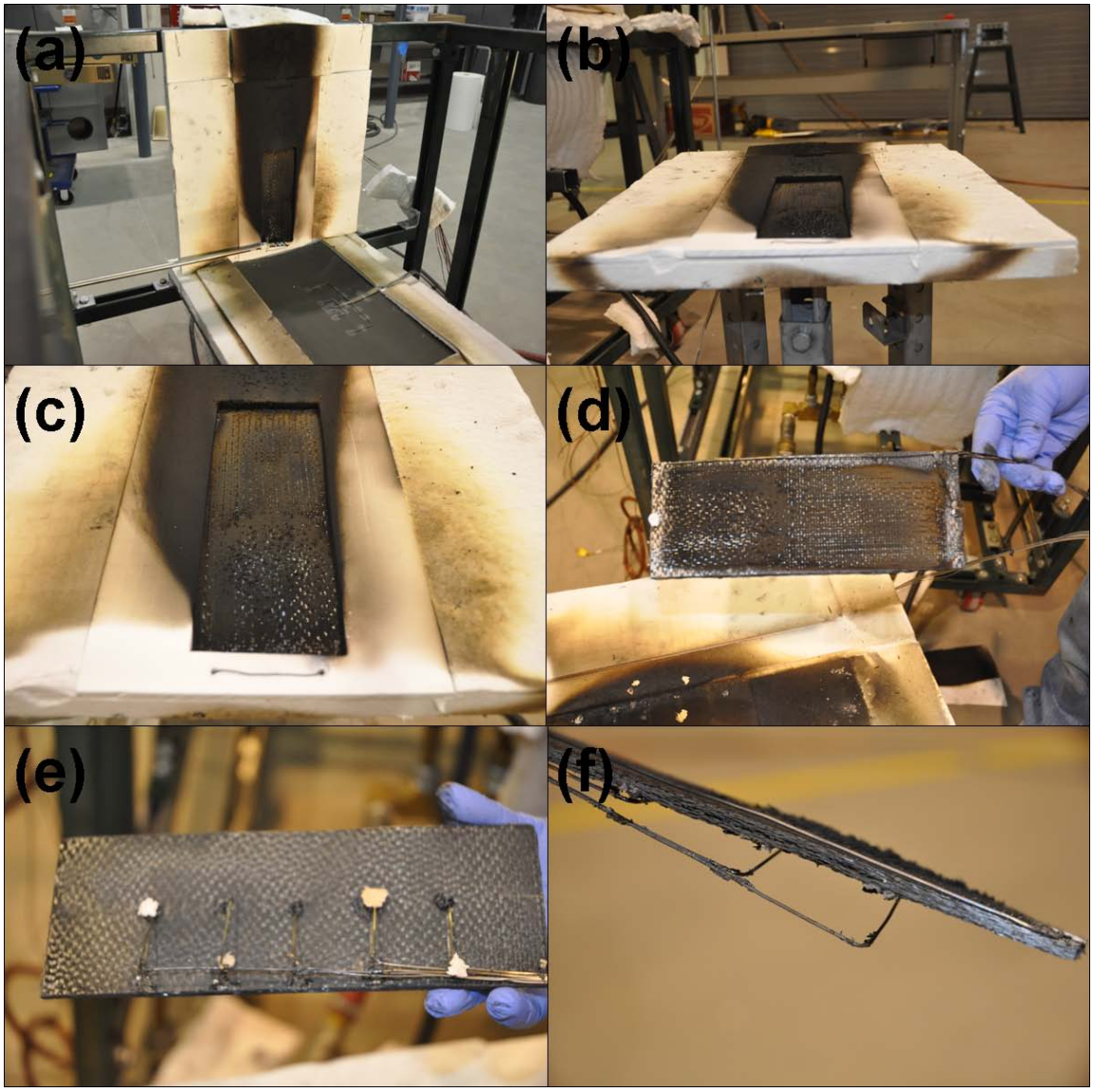

Figure A.12.2: (a) pre-test setup (b) post-test coupon front side, (c) post-test coupon front side, and (d) post-test coupon front side, (e) post-test coupon back side, and (f) post-test coupon side view

A.13 CYTEC BISMALEIMIDE FABRIC, PILOTED FLAME SPREAD (TEST 13)

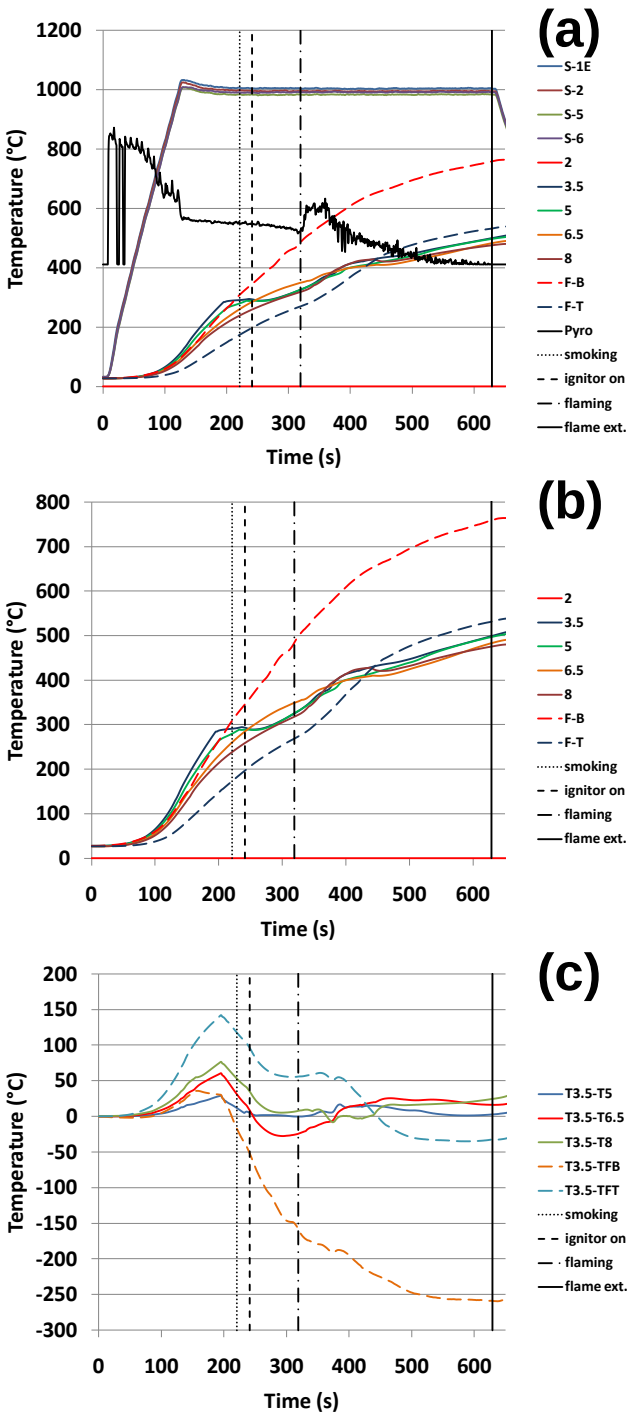

Figure A.13.1: (a) Shroud, pyrometer, and composite coupon temperature (°C) vs. elapsed time (s), (b) composite coupon temperature vs. elapsed time, and (c) composite coupon temperature differences (°C) with respect to thermocouple T3.5 (insulated side of coupon, 3.5 inches from bottom)

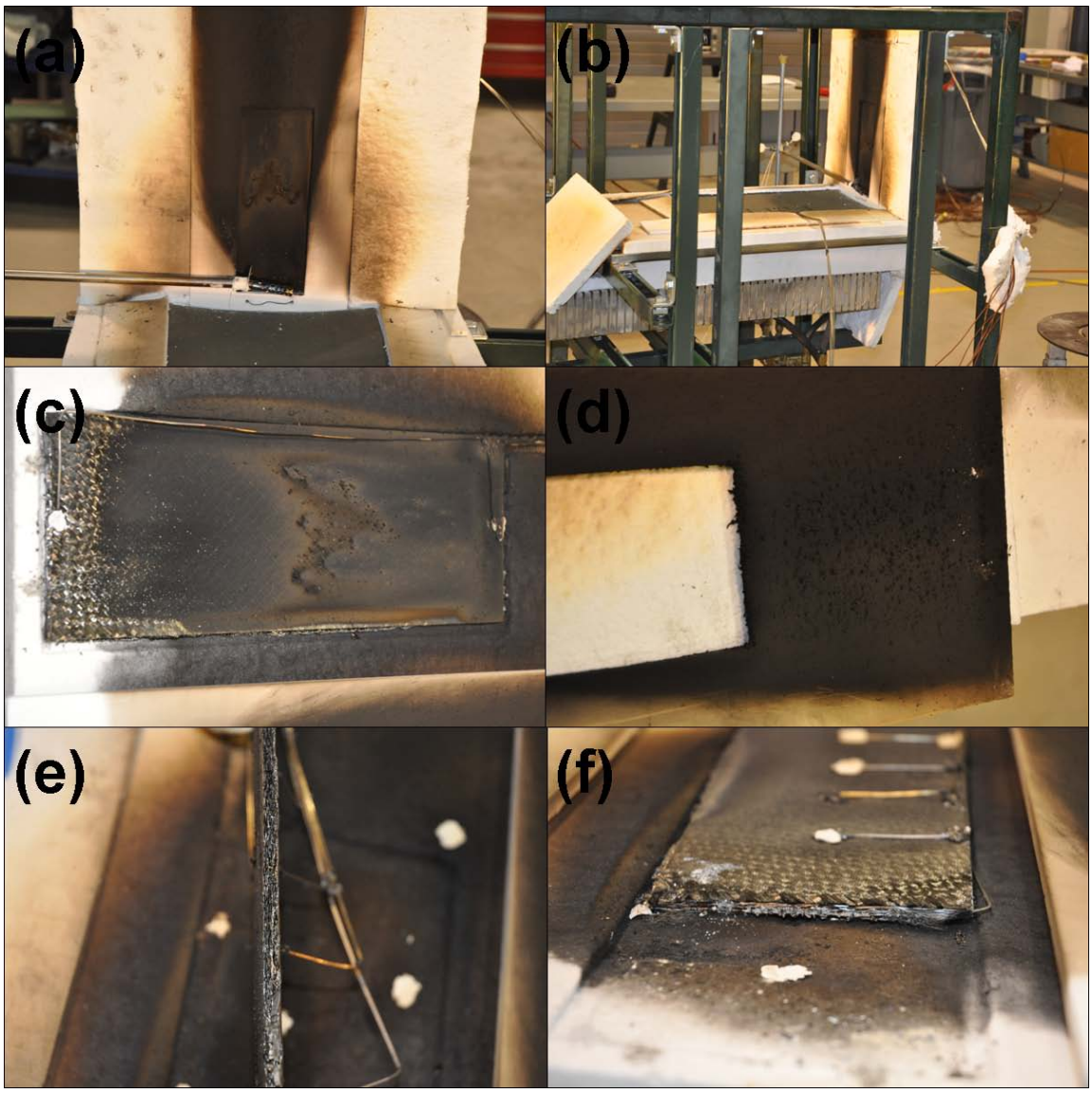

Figure A.13.2: (a) post-test setup, (b) post-test setup, (c) post-test coupon front side, (d) post-test mask residue, (e) post-test coupon side view, and (f) post-test coupon side view

A.14 CYTEC BISMALEIMIDE FABRIC, PILOTED FLAME SPREAD (TEST 14)

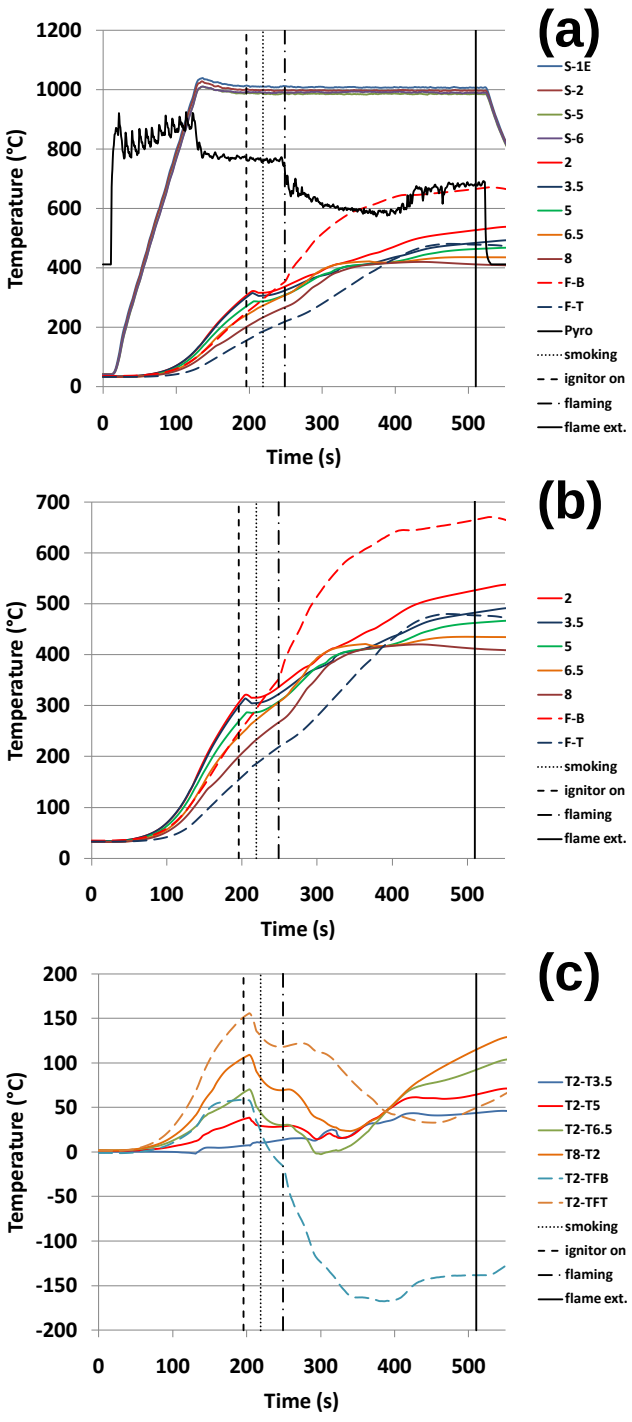

Figure A.14.1: (a) Shroud, pyrometer, and composite coupon temperature (°C) vs. elapsed time (s), (b) composite coupon temperature vs. elapsed time, and (c) composite coupon temperature differences (°C) with respect to thermocouple T2 (insulated side of coupon, 2 inches from bottom)

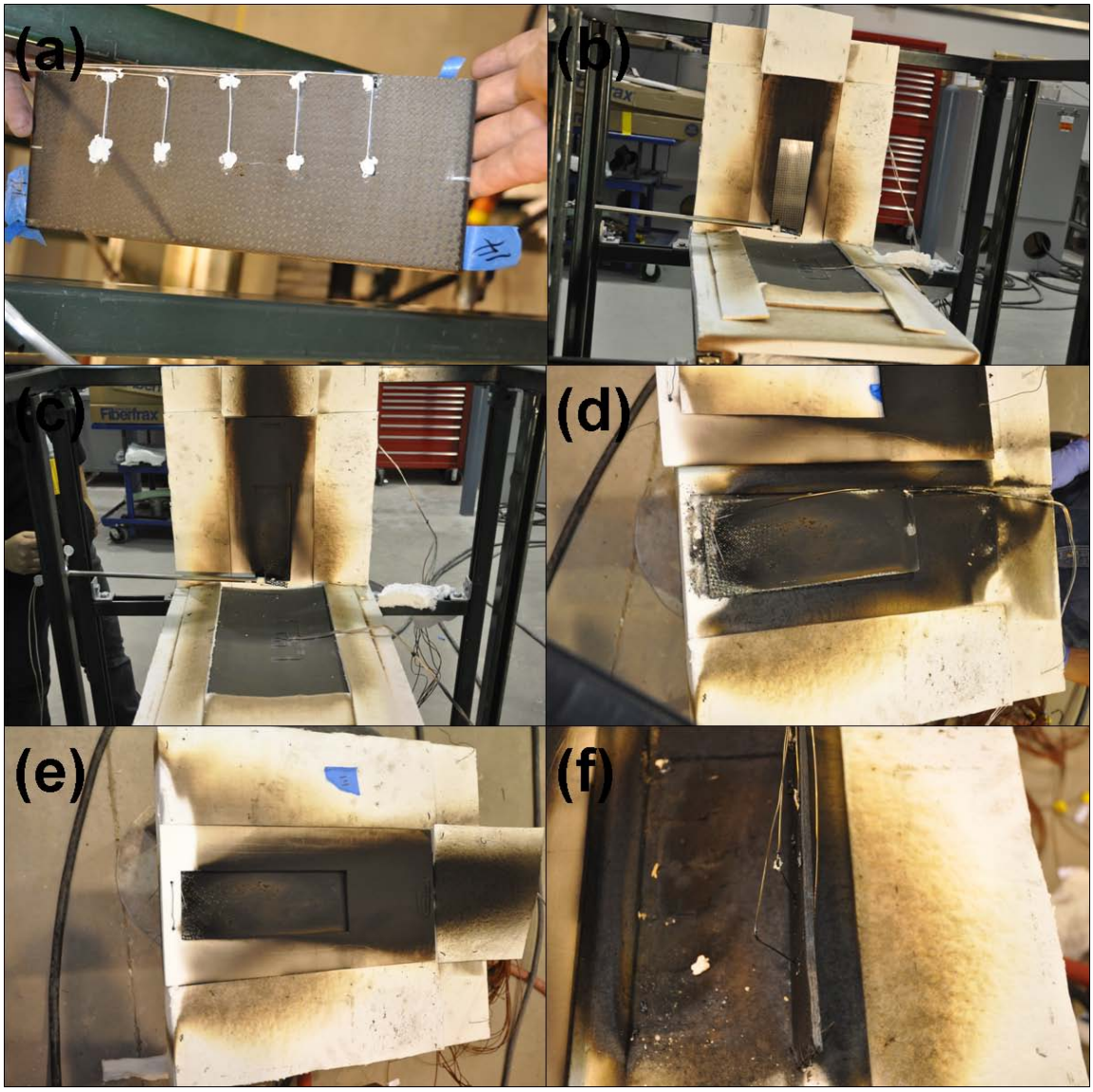

Figure A.14.2: (a) pre-test coupon back side (insulated), (b) pre-test setup, (c) post-test setup, (d) post-test coupon front side (irradiated), (e) post-test coupon front side, and (f) post-test coupon back side (insulated)

A.15 CYTEC EPOXY FABRIC, PILOTED FLAME SPREAD (TEST 15)

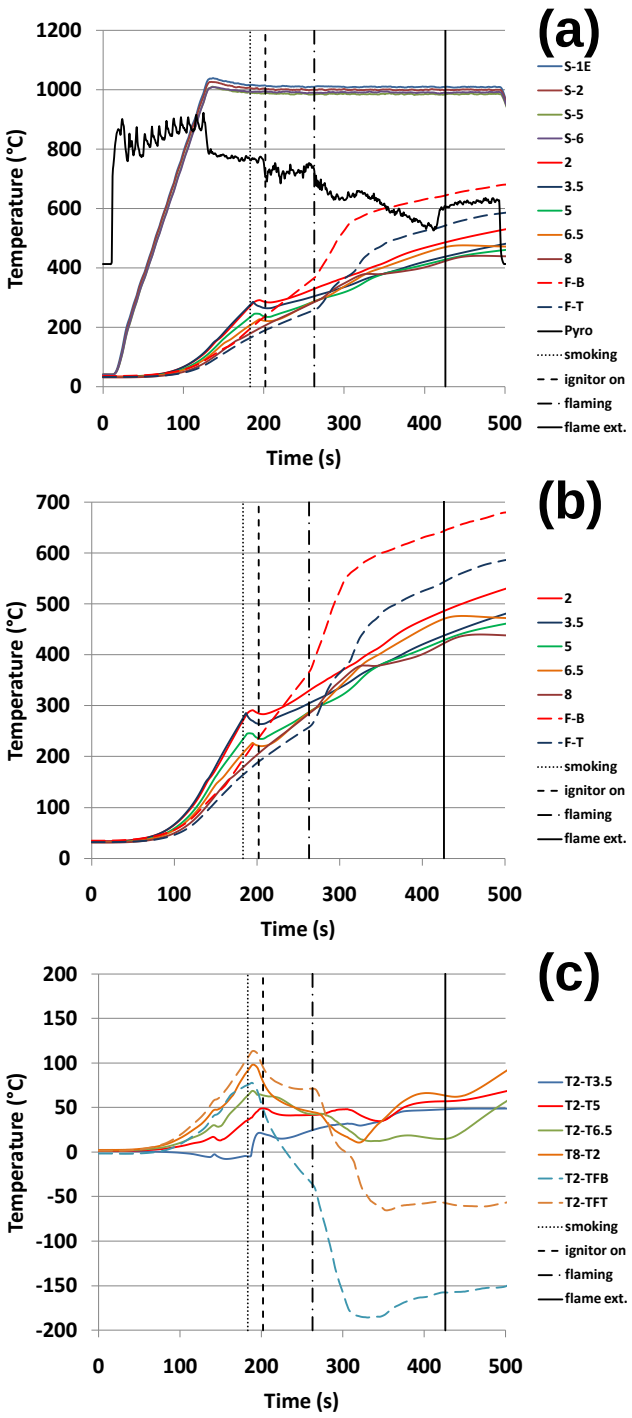

Figure A.15.1: (a) Shroud, pyrometer, and composite coupon temperature (°C) vs. elapsed time (s), (b) composite coupon temperature vs. elapsed time, and (c) composite coupon temperature differences (°C) with respect to thermocouple T2 (insulated side of coupon, 2 inches from bottom)

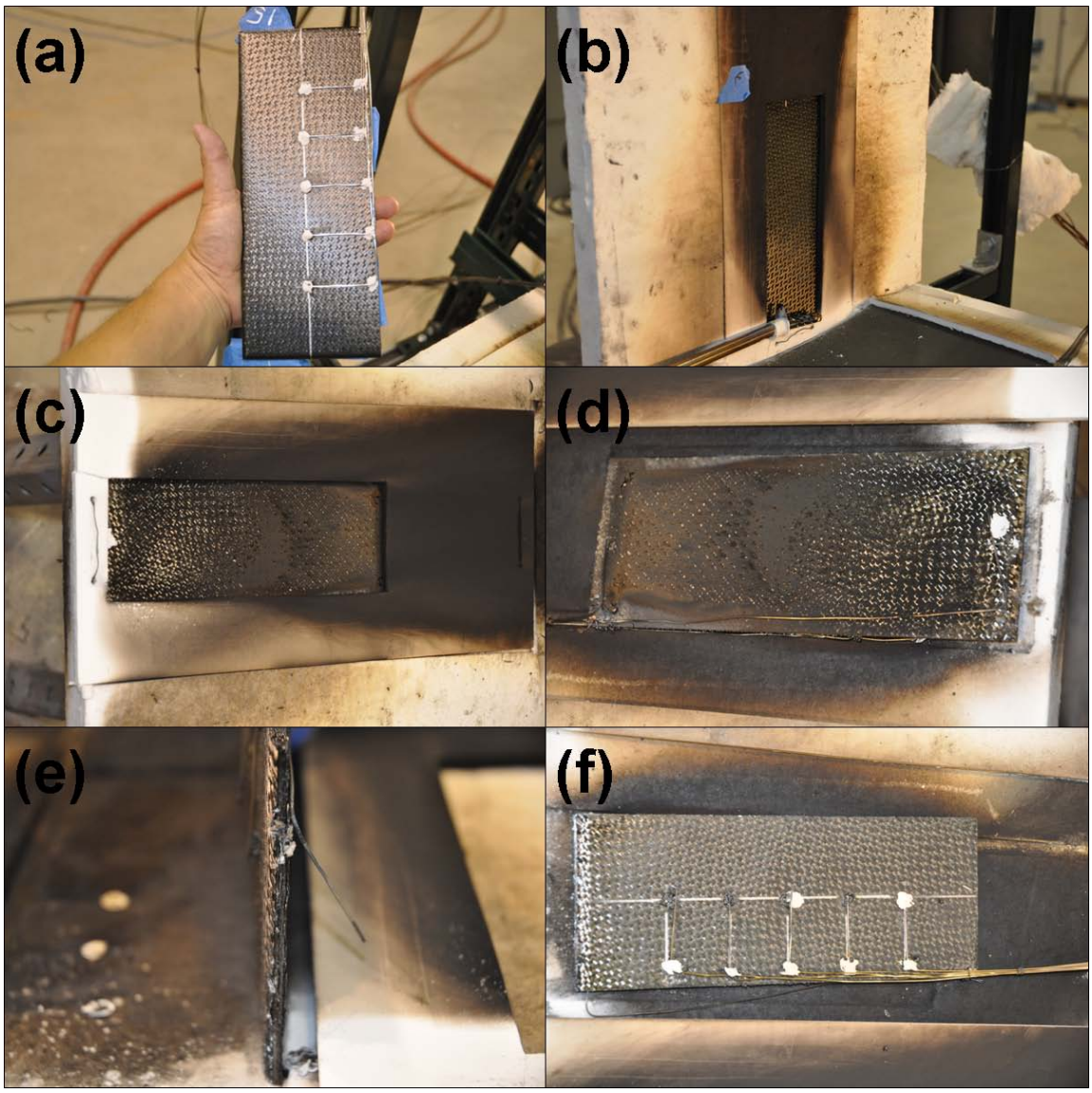

Figure A.15.2: (a) pre-test coupon back side (insulated), (b) pre-test setup, (c-d) post-test coupon front side (irradiated), (e) post-test coupon side view, and (f) post-test coupon back side

A.16 CYTEC EPOXY FABRIC, PILOTED FLAME SPREAD (TEST 16)

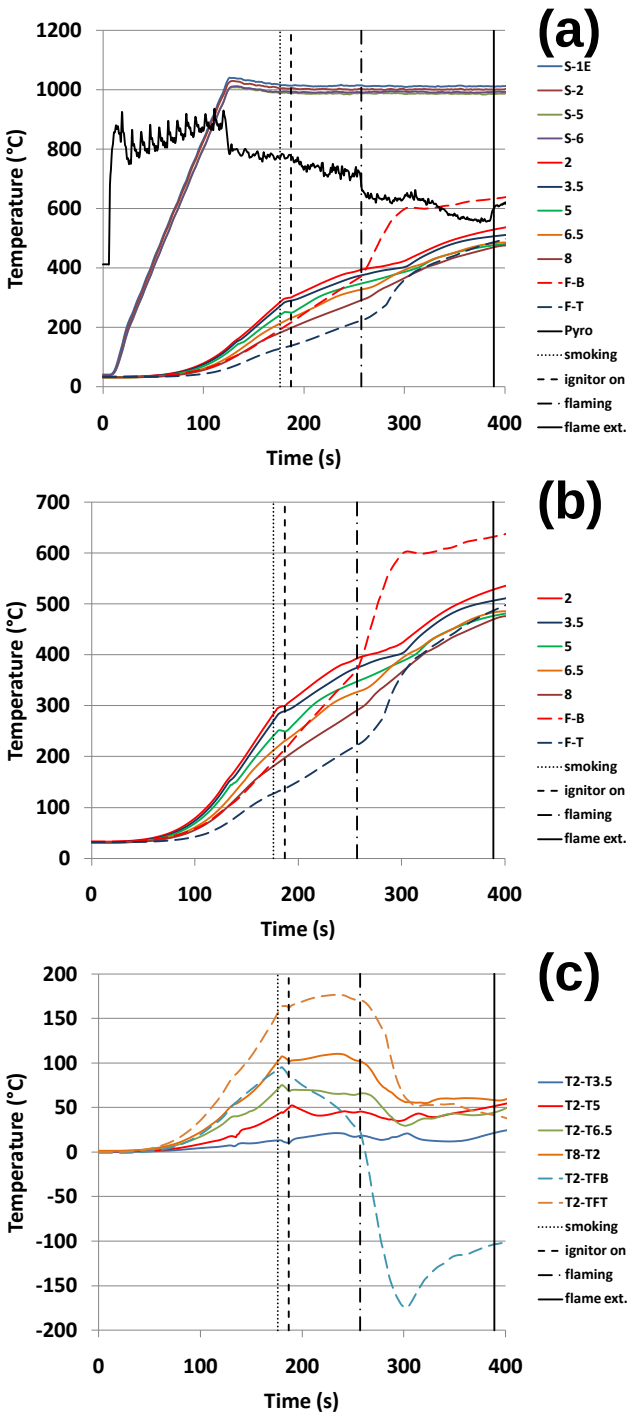

Figure A.16.1: (a) Shroud, pyrometer, and composite coupon temperature (°C) vs. elapsed time (s), (b) composite coupon temperature vs. elapsed time, and (c) composite coupon temperature differences (°C) with respect to thermocouple T2 (insulated side of coupon, 2 inches from bottom)

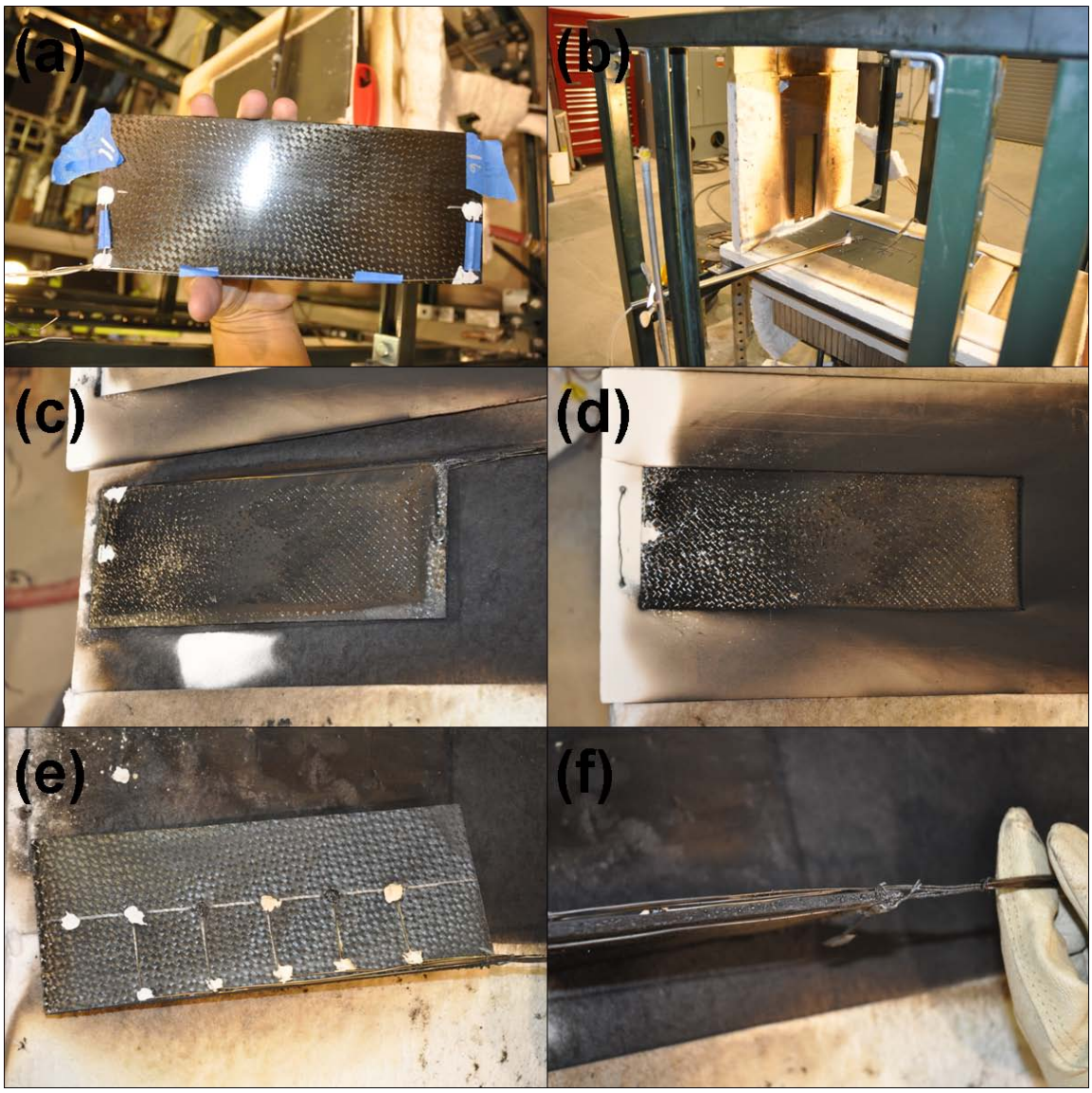

Figure A.16.2: (a) pre-test coupon front side (irradiated), (b) pre-test setup, (c-d) post-test coupon front side, (e) post-test coupon back side (insulated), and (f) post-test coupon side view

A.17 CYTEC BISMALEIMIDE TAPE, PILOTED FLAME SPREAD (TEST 17)

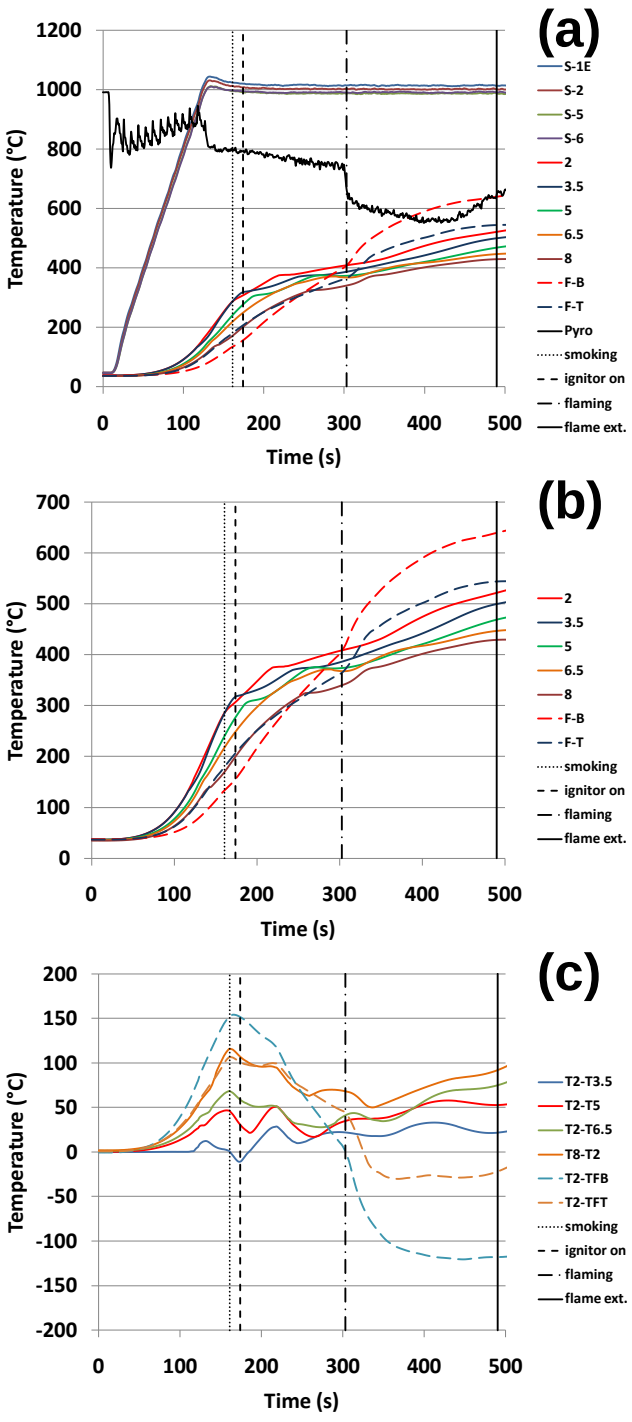

Figure A.17.1: (a) Shroud, pyrometer, and composite coupon temperature (°C) vs. elapsed time (s), (b) composite coupon temperature vs. elapsed time, and (c) composite coupon temperature differences (°C) with respect to thermocouple T2 (insulated side of coupon, 2 inches from bottom)

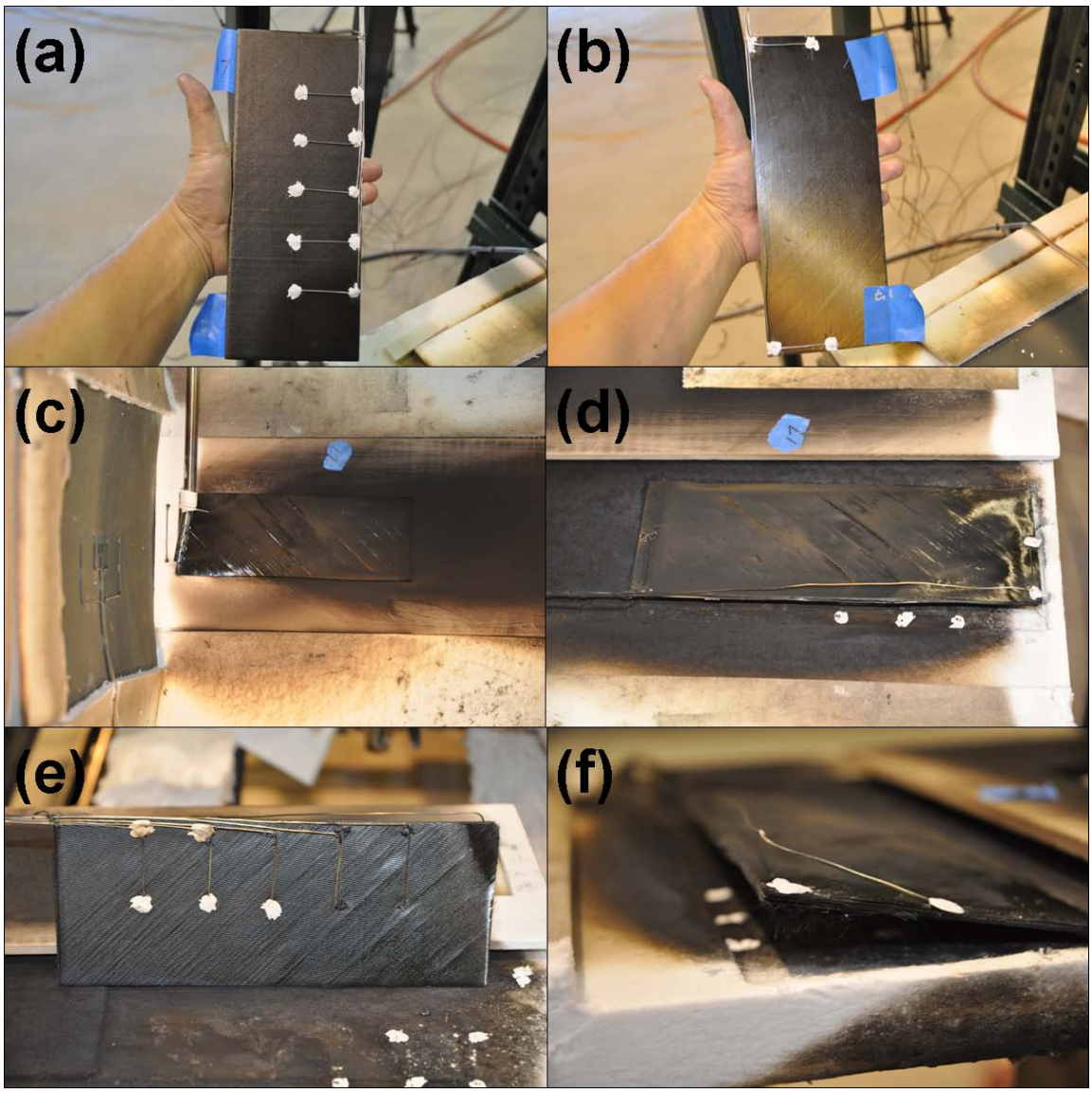

Figure A.17.2: (a) pre-test coupon back side (insulated), (b) pre-test coupon front side (irradiated), (c-d) post-test coupon front side, (e) post-test coupon back side, and (f) post-test coupon side view

A.18 CYTEC BISMALEIMIDE TAPE, PILOTED FLAME SPREAD (TEST 18)

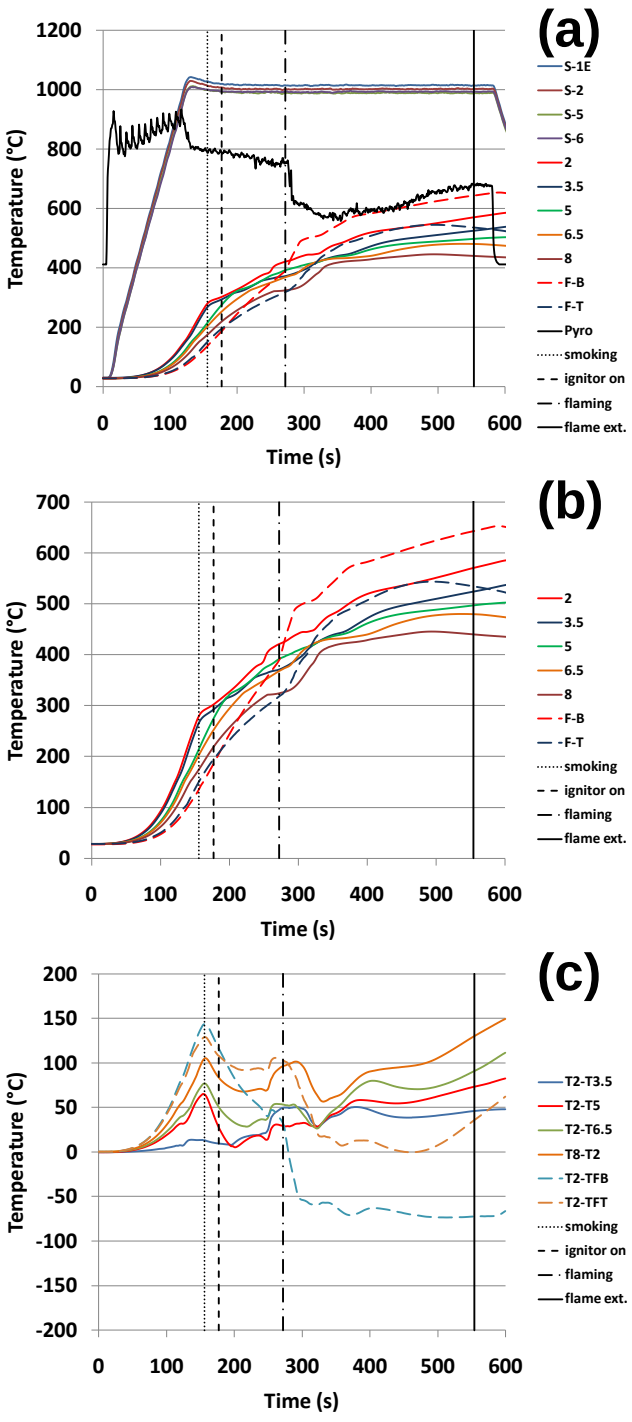

Figure A.18.1: (a) Shroud, pyrometer, and composite coupon temperature (°C) vs. elapsed time (s), (b) composite coupon temperature vs. elapsed time, and (c) composite coupon temperature differences (°C) with respect to thermocouple T2 (insulated side of coupon, 2 inches from bottom)

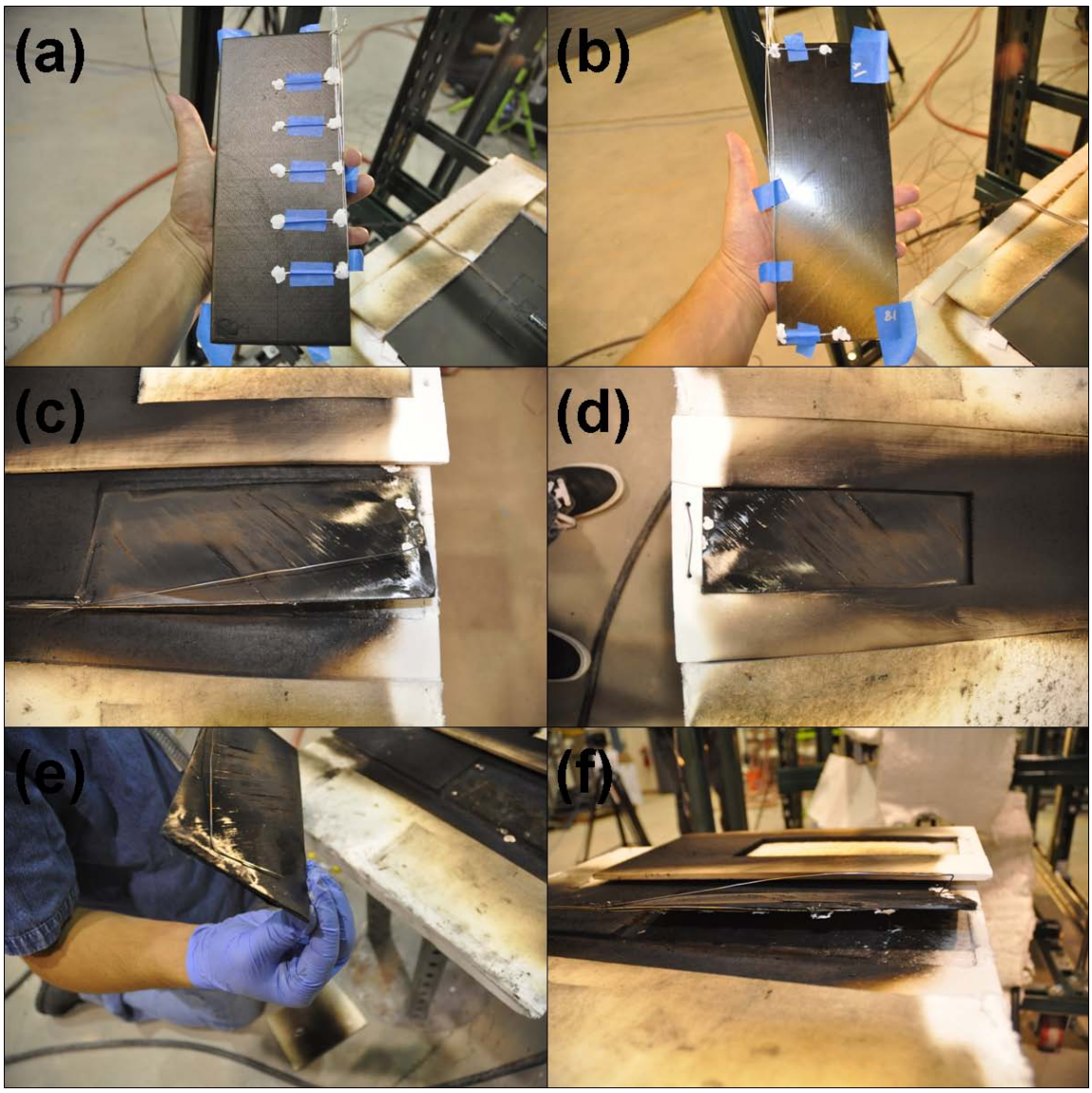

Figure A.18.2: (a) pre-test coupon back side (insulated), (b) pre-test coupon front side (irradiated), (c-d) post-test coupon front side, (e) post-test coupon back side, and (f) post-test coupon side view

A.19 CYTEC EPOXY TAPE, PILOTED FLAME SPREAD (TEST 19)

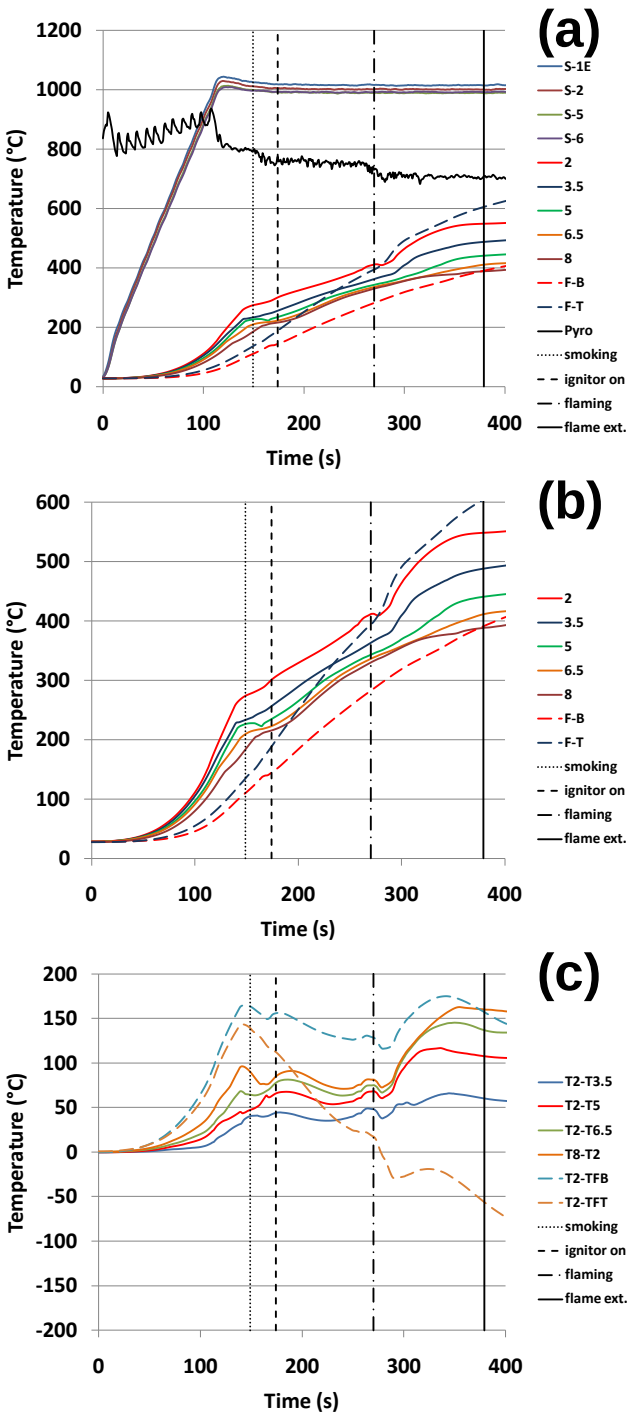

Figure A.19.1: (a) Shroud, pyrometer, and composite coupon temperature (°C) vs. elapsed time (s), (b) composite coupon temperature vs. elapsed time, and (c) composite coupon temperature differences (°C) with respect to thermocouple T2 (insulated side of coupon, 2 inches from bottom)

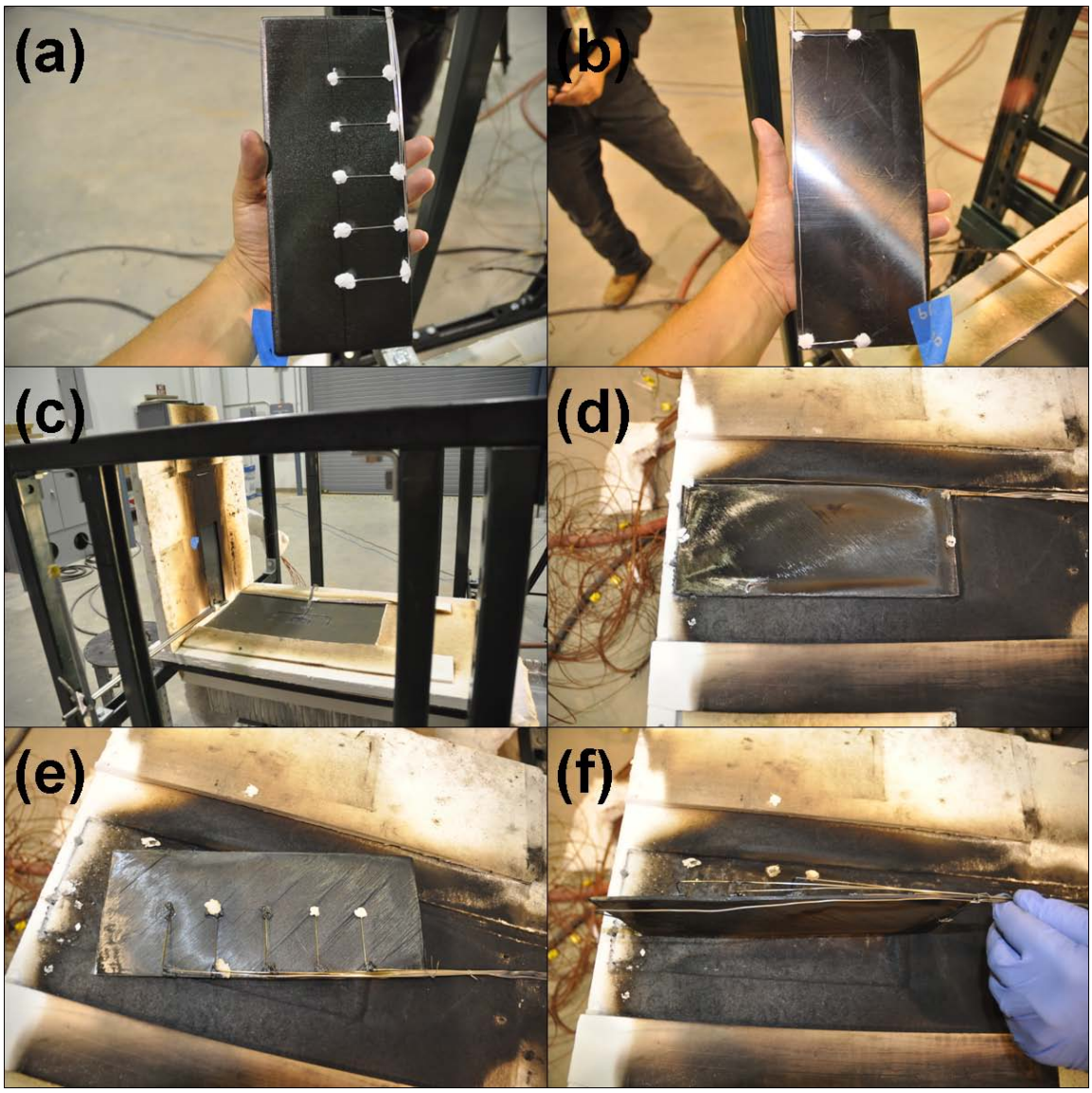

Figure A.19.2: (a) pre-test coupon back side (insulated), (b) pre-test coupon front side (irradiated), (c) pre-test setup, (d) post-test coupon front side, (e) post-test coupon back side, (f) post-test coupon side view

A.20 CYTEC EPOXY TAPE, PILOTED FLAME SPREAD (TEST 20)

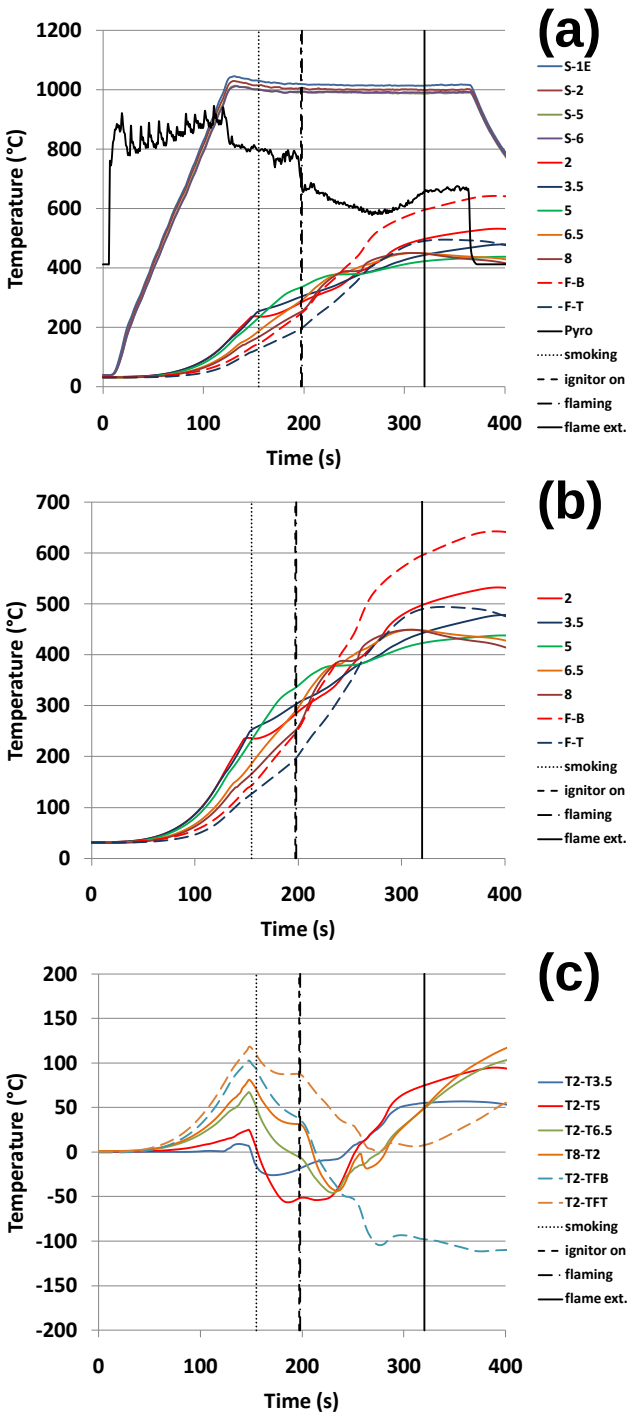

Figure A.20.1: (a) Shroud, pyrometer, and composite coupon temperature (°C) vs. elapsed time (s), (b) composite coupon temperature vs. elapsed time, and (c) composite coupon temperature differences (°C) with respect to thermocouple T2 (insulated side of coupon, 2 inches from bottom)

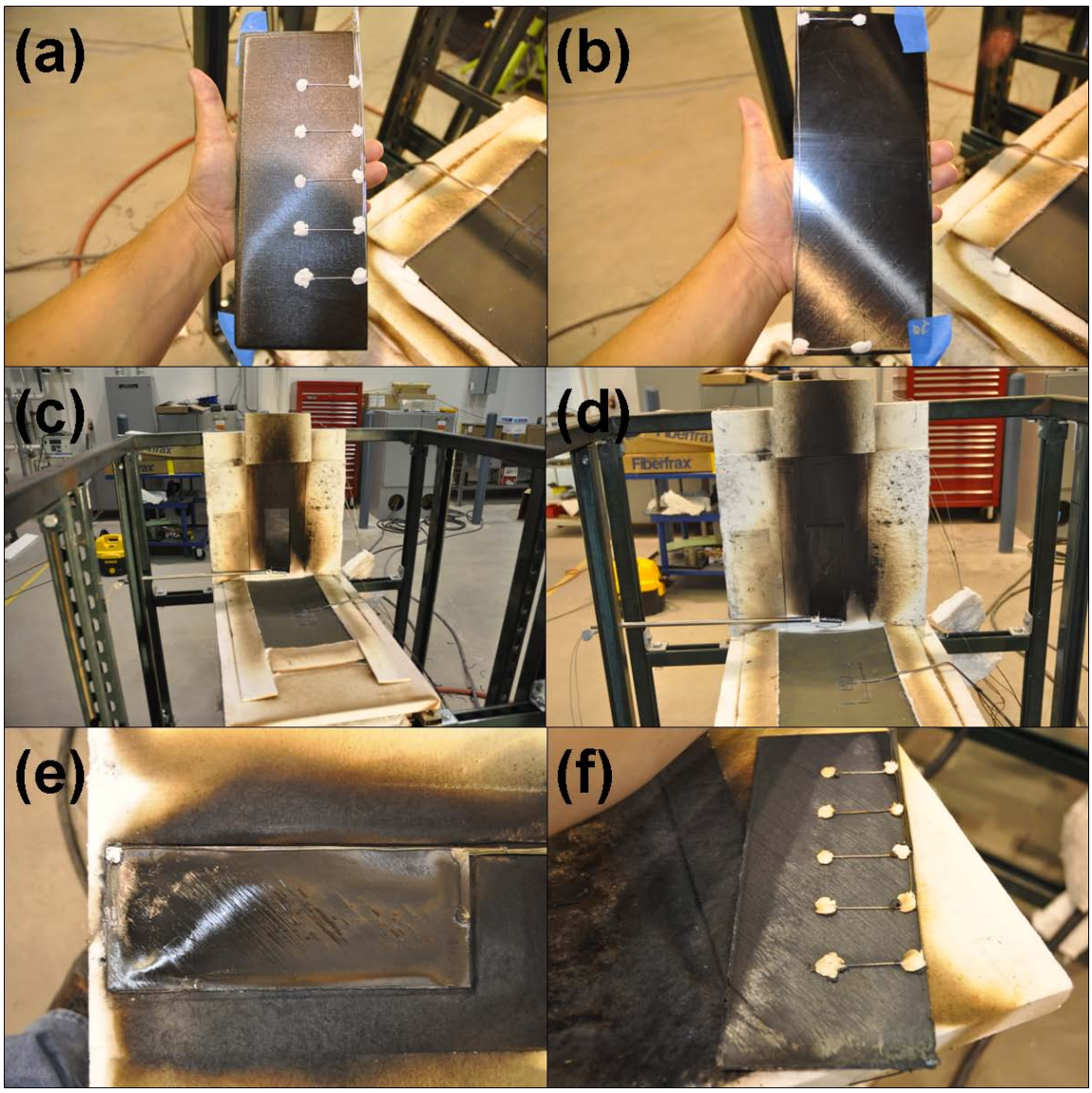

Figure A.20.2: (a) pre-test coupon back side (insulated), (b) pre-test coupon front side (irradiated), (c) pre-test setup, (d) post-test setup, (e) post-test coupon front side, (f) post-test coupon back side

DISTRIBUTION

Name of Person		Org. Number	
MS1135	Josh Hubbard	01532	
MS1135	Alex Brown	01532	
MS1135	Sylvia Gomez-Vasquez	01532	
MS1135	Ciro Ramirez	01533	
MS1135	Randy Watkins	01532	
MS0821	Anay Luketa	01532	
MS1135	Allen Ricks	01532	
MS1135	Tom Blanchat	01532	
MS1135	Jill Suo-Anttila	01532	
MS0836	Amanda Dodd	01514	
MS0828	Marty Pilch	01514	
MS0836	Roy Hogan	01514	
MS0826	Ken Erickson	01512	
MS0836	Chris Bourdon	01512	
MS0447	Jim Nakos	02127	
MS0836	Sheldon Tieszen	01541	
MS0899	Technical Library	9536	(electronic copy)


Sandia National Laboratories